Nanoscale

ROYAL SOCIETY OF CHEMISTRY

REVIEW

View Article Online
View Journal | View Issue

Cite this: *Nanoscale*, 2025, **17**, 18049

Materials, mechanisms, and emerging applications of electrochromic systems

Taimur Ahmed, *†[a,b] Aishani Mazumder, †[a] Sruthi Kuriakose,[c] Aditya Dubey,[d] Aaron Elbourne, [e] Jiawen Ren,[a] Vaishnavi Krishnamurthi,[a] Everson Kandare,[f] Irfan Haider Abidi,[a,b] Enrico Della Gaspera, [e] Sivacarendran Balendhran *[g] and Sumeet Walia *[a,b]

Electrochromic materials, capable of reversible color changes through electrochemical redox reactions, have garnered significant interest for diverse applications like smart windows, displays, and camouflage materials. However, their practical implementation hinges on tailoring material properties and dimensions to optimize device performance. This review critically examines the state-of-the-art in electrochromic technology, with a particular emphasis on the effects of material dimensionality and compositing strategies. We provide insights into various tunable approaches based on application requirements, enabling researchers to make informed choices for material combinations and dimensions. The review considers recent advancements, highlights major challenges and proposes potential future directions in the field. We discuss the prospects and trends in low-dimensional materials, such as nanostructures and two-dimensional (2D) materials, which offer unique opportunities for enhancing electrochromic properties and enabling new functionalities. Furthermore, we explore pathways towards commercialization, addressing the critical aspects of scalability, durability, and cost-effectiveness. By bridging the gap between fundamental research and practical applications, this review aims to stimulate further exploration and accelerate the development of next-generation electrochromic devices for a wide range of applications.

Received 16th May 2024,
Accepted 3rd June 2025

DOI: 10.1039/d4nr02098g

rsc.li/nanoscale

1. Introduction

Electrochromic materials have garnered significant attention due to their unique ability to reversibly change their optical properties, such as colour or transmittance, upon the application of an electrical stimulus.[1–7] This phenomenon, known as electrochromism,[8–11] has paved the way for a wide range of applications, including smart windows, displays, camouflage materials, and optoelectronic devices.[12,13] The underlying principle of electrochromism typically relies on charge or ion exchange between an electrolyte and a functional electrochromic material, resulting in a change in the material's oxidation state and, consequently, its optical properties.

Inorganic and organic materials, such as metal oxides, metal coordination complexes, viologens, and conjugated conducting polymers, have been extensively studied for their electrochromic properties. Inorganic materials, such as metal oxides and Prussian blue (PB), offer advantages such as high optical transmittance in the reduced state and reversible switching when deposited with good quality, making them attractive for applications requiring reversible switching and energy efficiency.[1,4,11,14] On the other hand, organic materials, including conjugated polymers, exhibit desirable characteristics such as multiple coloration states, fast switching speeds, and tailorable optical properties, enabling their use in displays and optoelectronic devices.[2,7]

To enhance and modulate the electrochromic performance of these materials, various strategies have been employed, including doping, nanostructuring, and compositing.[9,15–17] Nanostructuring, for instance, can increase ion diffusion rates, leading to higher coloration efficiencies with fewer charges and reduced overall energy consumption.[8,18] Additionally, compositing electrochromic materials with other functional materials, such as transparent conductive oxides or ion-conducting electrolytes, can improve their electrochemical and

[a]*School of Engineering, RMIT University, Melbourne 3000, Victoria, Australia. E-mail: taimur.ahmed@rmit.edu.au, sumeet.walia@rmit.edu.au*
[b]*Centre for Opto-electronic Materials and Sensors, RMIT University, Melbourne, VIC 3000, Australia*
[c]*Commonwealth Scientific Industrial Research Organisation, Sydney, NSW, Australia*
[d]*Integrated Photonics and Applications Centre (InPAC), School of Engineering, RMIT University, Melbourne, VIC 3000, Australia*
[e]*School of Science, RMIT University, Melbourne, VIC 3000, Australia*
[f]*Aerospace Engineering, School of Engineering, RMIT University, Melbourne, VIC 3082, Australia*
[g]*School of Electrical Engineering, The University of Melbourne, Melbourne, VIC 3010, Australia. E-mail: sbalendhran@unimelb.edu.au*
† These authors contributed equally.

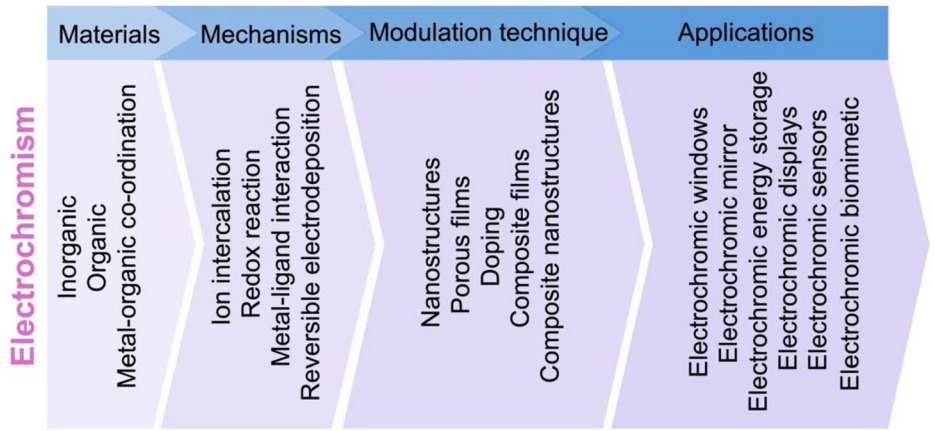

Fig. 1 Schematic representation of the mechanism, materials, modulation strategies and available applications in the realm of electrochromism.

optical properties, enabling further optimization for specific applications.[19–21]

The nature, degree, and reversibility of the colour/optical transmittance change in electrochromic materials are highly dependent on their intrinsic physical and chemical properties. Understanding these properties and their correlation with electrochromic performance is crucial for the rational design and development of efficient electrochromic devices. Moreover, the integration of these materials into functional devices requires consideration of factors such as scalability, durability, and cost-effectiveness, which can pose significant challenges for large scale practical applications.

Recently, Chen *et al.*[22] reviewed the historical development and latest advancements of zinc anode-based electrochromic devices, highlighting their multifunctional applications, including dual-band tunability and energy retrieval. Similarly, Zhao *et al.*[23] examined the integration of electrochromism and energy storage functionalities, addressed inherent contradictions between these two functions and proposed design strategies for electrochromic energy storage devices. Stability challenges in electrochromic materials, specifically using plasmonic materials to enhance stability, are reviewed by Liu *et al.*[24] and offer detailed techniques for structure and morphology engineering. In comparison with these recent reviews, our work focuses on the impact of material dimensionality and compositing strategies on the performance of electrochromic devices, with an emphasis on optimizing these parameters for practical applications. We provide insights into various tunable approaches based on application requirements, discuss recent advancements, and highlight major challenges in the field. Additionally, our review presents a broad overview of electrochromic materials and their coloration mechanisms in the visible and near infrared (NIR) ranges, while also offering detailed insights into property modulation using different tuning strategies. The review also discusses the applicability of electrochromic devices across various domains and explores their prospects in emerging applications. This review endeavours to expedite the advancement of next-generation electrochromic technologies by connecting fundamental research with practical applications. Fig. 1 outlines the scope of the review, which considers materials that exhibit electrochromic behaviour, the mechanisms responsible for this phenomenon, available modulation techniques and current potential applications.

2. Electrochromic materials

Materials exhibiting inherent electrochromic properties can be divided into organic, inorganic, hybrid organic/inorganic and metal oxide framework domains. The electrochromic efficiency of such materials is defined by several parameters. For instance, colouration efficiency (CE), often termed electrochromic efficiency, which is the unit charge-induced change in optical density (OD) of a material at a particular wavelength and denotes the number of charges required to induce a colour change.[16] The CE and OD of the electrochromic material are defined by two equations:[8]

$$\mathrm{CE} = \frac{\Delta \mathrm{OD}}{\Delta Q} \tag{1}$$

$$\mathrm{OD} = \log \frac{T_\mathrm{b}}{T_\mathrm{c}} \tag{2}$$

where Q is the intercalated ionic charge per unit and T_b and T_c are the transmittance changes in the bleached and coloured states, respectively.[8] As such, a higher CE indicates lower charge consumption, thus higher energy efficiency.[16] Another important parameter is the switching time, *i.e.* the response speed of the material to attain a 10% to 90% change in its transmittance between the coloured and bleached states. The availability of increased surface area and pathways for effective ion diffusion can allow for shorter response times.[18] Another important parameter for the real-life application of any EC device is its high cycling stability, where each cycle comprises colouration and bleaching.[18] For example, an electrochromic

device (ECD) being cycled on an average of 2 cycles per day requires a cycling stability of 14 600 cycles to function over 20 years.[25] A high cycling stability and enhanced switching times are crucial factors for applications of ECDs.[26] Furthermore, the characterization of electrochromic materials is crucial for assessing their characteristics, performance, and potential applications. There are several characterization techniques usually adopted to investigate electrochromic materials. Among these techniques, the spectroelectrochemical technique utilizes electrochemical and spectroscopic methods to measure changes in the optical properties of electrochromic materials under applied potential and enable the real-time monitoring of the electrochromic response. It is also very effective at probing both different oxidation states and the location of redox centers in electrochromic materials, such as conducting polymers.[27–29] An alternative method involves observing changes in the vibrational energy levels of an electrochromic material during an electrochemical reaction by using vibrational spectroscopy techniques, such as Fourier transform infrared (FTIR) and Raman spectroscopy. This enables the monitoring of structural and conformational changes occurring in the material.[30–32] The charge transport mechanisms, ion diffusion processes and interfacial properties of electrochromic materials can be assessed by electrochemical impedance spectroscopy.[33–35] More importantly, the coloration efficiency, electrochromic contrast and optical modulation of an electrochromic material can be evaluated by measuring optical transmittance and absorbance in different optical bands ranging from ultraviolet to near-infrared spectral bands.[28,32] Additional nano-structural and compositional analysis, such as topographic and mechanical properties, physiochemical defects, grain boundaries and interfaces within the synthesised electrochromic materials can be carried out by atomic force microscopy, X-ray diffraction, transmission electron microscopy and scanning electron microscopy.[36,37] As such, these techniques collectively provide comprehensive insights into the physical, chemical, and electrochemical properties of electrochromic materials and enable optimization for their applications in smart windows, displays and energy storage devices.

This section covers various electrochromic materials reported in the literature and assesses their key performance parameters. A list of various organic, inorganic and organic–inorganic state-of-the-art electrochromic materials is provided in Table 1.

2.1. Inorganic materials

Transition metal oxides (TMOs) comprising cathodic and anodic EC oxides are some of the most investigated inorganic EC materials.[38,39] The operating principle of cathodic and anodic components is complementarity, as ion intercalation results in colouration in cathodic TMOs whereas upon intercalation anodic TMOs undergo bleaching/de-colouration.[39] Cathodic oxides are comprised of oxides of molybdenum (Mo), tungsten (W), tantalum (Ta) and titanium (Ti), whereas oxides of chromium (Cr), manganese (Mn), nickel (Ni), iron (Fe), cobalt (Co), rhodium (Rh) and iridium (Ir) are anodic in nature.[39] Interestingly, some TMOs such as vanadium (V)-based metal oxides have a combination of both cathodic and anodic attributes.[39] The aforementioned EC oxides are widely studied due to their improved photochemical stability, long cycle life, better optical memory and higher environmental stability.[1,40] Amongst the cathodic TMO family, tungsten trioxide (WO_3), molybdenum trioxide (MoO_3) and nickel oxide (NiO) have the highest reported CE values.[41] Of these TMOs, WO_3 is extensively studied due to its superlative colouration efficiency and stability over other TMOs.[42] However, TMOs like WO_3 can be costly to manufacture due to the rarity of W metal, whereas NiO often suffers from poor ion diffusion and low electrical conductivity.[1,38] Compared to WO_3, MoO_3 is a less dense material due to its layered crystal structure, which can improve the energy efficiency of applications.[43] Anodic electrochromic oxides of Ir, like many cathodic oxides, display high values of CE, but can be expensive, despite being alloyed with cost-effective materials like tin (Sn) and Ta.[39] Despite several advantageous features, TMOs suffer from slower switching speeds, high redox potential and possess only a single colouration state, which can be ineffective for many EC applications.[15,44,45] Other than TMOs, in recent years, MXenes have been garnering a lot of interest based on their electrochromic properties with the $Ti_3C_2T_x$ variant being widely investigated for its electrochromic properties. Although MXenes have demonstrated unprecedented electrochromic properties,[46] stacking and affinity for rapid oxidation remain challenging for these materials.[47]

2.2. Organic materials

Electrochromic redox mechanisms are commonly seen in organic materials such as 1,1′-disubstituted-4,4′-dipyridinium salts (*i.e.*, viologens), commonly known as non-polymerics and conducting polymers also known also polymerics, such as polyaniline (PANI), polypyrrole (PPy), polythiophene and their derivatives.[2,16,39] Viologens are stable and colourless in their EV^{2+} state and exhibit colouration when undergoing the reduction process.[39] They demonstrate high transmittance modulation and CE, fast colouration, and rapid switching.[2,48,49] However, unlike other organic EC materials, they have a single colouration state and demonstrate slow ionic diffusion in electrolytes.[48,49]

One of the key advantages of organic conducting polymers such as polypyrrole, PANI, poly(3,4-ethylenedioxythiophenes) (PEDOT) is the presence of multiple colouration states, which can be beneficial for applications such as displays. Furthermore, they are cheaper, have a simple synthesis mechanism, and demonstrate high CE, low oxidation potential and a rapid response speed.[3,38,44] Despite their desirable electrochromic properties, the non-uniformity of films produced from organic conducting polymers results in low cycling stability, as reported by Hasani *et al.*[7] Also, the susceptibility of organic polymers to the ultraviolet (UV) region of the EM spectrum and their band-shifting characteristics make them less suited as standalone materials for applications like EC smart

Table 1 Inorganic and organic materials and their electrochromic properties. Abbreviations used in the table: TTAz = 1-phenyl-2-[4-(2,20:50,200-terthien-30-ylmethoxy)phenyl]diazene, TTCo = 4-(2,20:50,200-terthien-30-ylmethoxy)-2*H*-chromen-2-one, TTFlo = methyl 2-[3-oxo-6-(2,20:50,200-terthien-30-ylmethoxy)-3*H*-xanthen-9-yl]benzoate, ITO = indium tin oxide

Material	Colouration efficiency ($cm^2\ C^{-1}$)	Switching time τ_b/t_b = bleach time, τ_c/t_c = colour time	Optical modulation DT = $T_b - T_c$	Optical density	Cycling endurance
Tungsten trioxide (WO_3)	154 at 633 nm (ref. 63)	τ_b = 1 s, τ_c = 1 s at 633 nm (ref. 63)	97.8% at 633 nm (ref. 25)	3.676 at 555 nm (ref. 64)	20 000 cycles at 633 nm (ref. 25)
Molybdenum trioxide (MoO_3)	84.97 at 550 nm (ref. 10)	τ_b = 0.11 s, τ_c = 0.14 s (ref. 10)	45.5% at 600 nm (ref. 65)	0.8614 at 600 nm (ref. 65)	1200 cycles (ref. 66)
Titanium dioxide (TiO_2)	260.71 at 600 nm (ref. 67)	τ_c = 2.37 s, τ_b = 1.7 s at 600 nm (ref. 67)	67% at 600 nm (ref. 68)	2.19 at 600 nm (ref. 67)	1500 cycles from 200–800 nm (ref. 69)
Tantalum pentoxide (Ta_2O_5)	10 at 700 nm (ref. 70)	Not mentioned	56.7% at 550 nm (ref. 71)	Not mentioned	300 cycles at 700 nm (ref. 70)
Cobalt tetraoxide (Co_3O_4)	27 at 633 nm (ref. 72)	τ_b = 0.68 s, τ_c = 0.5 s at 633 nm (ref. 73)	42% at 633 nm (ref. 74)	1.27 at 633 nm (ref. 73)	4500 cycles at 633 nm (ref. 72)
Manganese dioxide (MnO_2)	28 at 680 nm (ref. 75)	τ_b = 12.3 s, τ_c = 8.1 s at 680 nm (ref. 75)	1% at 680 nm (ref. 75)	Not mentioned	1000 cycles at 680 nm (ref. 75)
Nickel oxide (NiO)	42 at 550 nm (ref. 76)	τ_c = 1.55 s, τ_b = 1.22 s at 630 nm (ref. 77)	82% at 550 nm (ref. 76)	1.06 at 630 nm (ref. 77)	3000 cycles at 550 nm (ref. 78)
Ferric oxide (Fe_2O_3)	28 at 550 nm (ref. 79)	Not mentioned	12% at 550 nm (ref. 79)	~0.10 at 700 nm (ref. 80)	250 cycles at 550 nm (ref. 79)
Rhodium trioxide (Rh_2O_3)	29.1 at 700 nm (ref. 81)	τ_c = 6 s, τ_b = 2 s at 600 nm (ref. 82)	76.6% at 700 nm (ref. 81)	0.723 at 700 nm (ref. 83)	25 000 at 700 nm (ref. 83)
Vanadium pentoxide (V_2O_5)	53.1 at 415 nm (ref. 84)	τ_c = 86.7 ± 2.3 ms, τ_b = 82.5 ± 2.9 ms at 430 nm (ref. 5)	49.8% at 430 nm (ref. 5)	Not mentioned	100 cycles at 430 nm (ref. 5)
Prussian Blue (PB)	131.5 at 700 nm (ref. 11)	τ_b = 1.0 s, τ_c = 2.4 s at 680 nm (ref. 85)	73.62% at 633 nm (ref. 86)	1.34 at 633 nm (ref. 86)	20 000 cycles at 690 nm (ref. 87)
Cobalt hexacyanoferrate (CoHCF)	28.2 at 550 nm (ref. 88)	τ_c = 31 s, τ_b = 122 s at 550 nm (ref. 88)	80% at 550 nm (ref. 88)	Not mentioned	100 cycles at 550 nm (ref. 88)
Molybdate hexacyanoferrate (MoOHCF)	46.93 at 480 nm (ref. 38)	Response time = 2.1 s (ref. 38)	48% at 480 nm (ref. 38)	0.53 at 480 nm (ref. 38)	300 cycles (ref. 38)
Ruthenium purple	134.5 at 580 nm (ref. 89)	τ_c = 0.92 s, τ_b = 0.5 s at 545 nm (ref. 89)	54.8% at 545 nm (ref. 89)	Not mentioned	50 cycles at 545 nm (ref. 89)
Polypyrrole (PPy)	23.33 at 630 nm (ref. 90)	τ_c = 1.5 s, τ_b = 2 s at 630 nm (ref. 90)	34.68% at 630 nm (ref. 90)	0.28 at 630 nm (ref. 90)	Not mentioned
Polyaniline (PANI)	216.3 at 700 nm (ref. 44)	τ_c = 0.6 s, τ_b = 0.6 s at 700 nm (ref. 91)	62.4% at 700 nm (ref. 44)	Not mentioned	400 cycles at 700 nm (ref. 44)
PTTAz[92]	Not mentioned	2.5 s at 500 nm 0.7 s at 770 nm 2 s at 1220 nm	28% at 500 nm 25% at 770 nm 64% at 1220 nm	Not mentioned	250 cycles
PTTCo[92]	Not mentioned	2 s at 475 nm 0.5 s at 740 nm 1 s at 1200 nm	25% at 475 nm 32% at 740 nm 63% 1200 nm	Not mentioned	250 cycles
PTTFlo[92]	Not mentioned	0.4 s at 496 nm 0.5 s at 1280 nm	16% at 496 nm 50% at 1280 nm	Not mentioned	250 cycles
PProDOT-$(CH_2OEtHx)_2$/ITO[93]	845 at 550 nm	0.6 s	>71%	Not mentioned	>5000 cycles
PProDOT-$(CH_2OEtHx)_2$ single walled carbon nanotubes[93]	573 at 550 nm	3.4 s	66%	Not mentioned	2500 cycles
PProDOP/PProDOT-Hx_2 [94]	224/519	0.9 s/0.6 s	>60%/>75%	Not mentioned	Not mentioned
Conducting polymers[95] [Cl-Bz-ProDOT/Br-Bz-ProDOT/NH_2-Bz-ProDOT]	209–692	8 ≤ 1 s	60% at 575 nm	Not mentioned	>10 000 cycles
N,*N*-Bis(4-aminophenyl)-*N*′,*N*′-bis(4-*tert*-butylphenyl)-1,4-phenylenediamine[96]	216 at 983 nm	τ_b = 2.4 s, τ_c = 2.9 s at 983 nm	90% at 778 nm	Not mentioned	>500 cycles

windows.[38] However, this limitation can be readily mitigated by incorporating a UV filter, such as a polyethylene terephthalate (PET) encapsulant or an indium tin oxide (ITO) substrate, which effectively blocks UV radiation and ensures the long-term stability and performance of the EC device.

2.3. Inorganic and organic compounds

Transition metal hexacyanoferrates (PB and its analogues) commonly known as Prussian blue analogues (PBA) are a class of metal–organic co-ordinated compounds[50] that undergo optical alterations under an applied bias.[38,51,51] PBA, also known as metal hexacyanoferrates (MHCFs), are composed of hexacyanoferrate compounds and a metal salt where the colouration obtained is dependent on the metal salts.[38] The structure comprises transition metals such as Ni, Cu, Co, Mo, indium (In), Cr, Fe, zinc (Zn) and vanadium (V).[38] PB and its analogues are low-cost materials with high redox reversibility, a large transmittance and operate at low voltages, making them energy efficient.[4,38] However, one of the challenges with PB is the lack of cycling stability due to weak adhesion to substrates.[4] This can make it challenging to integrate PBs into commercial electrochromic devices.[4]

2.4. Metal–organic frameworks (MOFs)

MOFs are composed of organic ligands and metal centers that offer enhanced conductivity, ion mobility, and structural stability.[52] They are a promising choice for next generation EC materials due to their tuneable microstructures. However, MOF-based EC materials reported so far have poor conductivity (less than 10^{-10} S cm^{-1}) that negatively affects their electrochromic performance.[52] Therefore, it is necessary to find a sweet spot between the electron transfer rates and ionic migration to improve the overall performance of the device. Recent reports have shown that the combination of MOFs with conductive polymers or transition metal oxides like WO_3, NiO, and V_2O_5,[53–56] can significantly improve optical modulation, switching speeds, and long-term stability. The addition of viologen derivatives to MOF structures creates multi-stimuli-responsive materials, which can change colour under various stimuli, such as electricity, light, and heat.[54,57–59] These materials show promise for applications in sensors, displays, and ink-free printing. The development of K-rich Prussian blue (PB) films using electrodeposition with amine group surface termination on ITO substrates gives a higher stability performance.[60,61] K-rich PB films ensure the homogeneous growth of the PB film and improve its cycling stability, achieving 87% retention of charge density after 1000 cycles.[61] This amine-terminated ITO surface helps to reduce lattice vacancies in the PB lattice, preventing film cracking and delamination.[61] Hybrid materials like surface-anchored metal–organic frameworks (SurMOFs)[62] show promise for overcoming limitations in inorganic/organic EC materials. SurMOFs are created by growing MOFs directly on substrates and they can exhibit electrochromic properties from both the metallic node and organic linker. A recent report on perylenediimide (PDI) linkers showed that they exhibited EC when reduced by lithium insertion or different electrolytes. These PDI-SurMOFs had improved stability, allowing further electrochromic characterization, opening up the possibility of designing near-infrared electrochromic materials, which are useful for energy-efficient smart windows.[62] However, challenges remain in the synthesis of MOF-based EC thin films, as traditional methods often result in powder forms that could possibly complicate film formation. Novel techniques like solvothermal, doctor blade, and electrochemical deposition have been proposed to address this problem, but the relationship between film structure and electrochromic properties is still under investigation.[52] While significant progress has been made, issues such as long-term stability, cost-effectiveness, and scalability still need to be addressed for the use of MOFs in practical applications in smart windows and other electrochemical devices.

3. Mechanisms in electrochromic devices

In an electrochromic device, an electric field-driven redox reaction is used to manipulate the optical properties of materials, resulting in visible colour changes. This redox reaction can be initiated in materials through ion insertion/extraction into the host lattice, reversible electrodeposition, metal–ligand interactions, proton-coupled charge transfer or through charge transfer processes within the material. A detailed discussion of each of these processes is outlined in the sub-sections below.

3.1. Ion intercalation

Ion intercalation is the reversible insertion of ions into a host material,[97,98] where the intercalated ions can be removed from the host using a reversal of electrical stimulus. For example, if intercalation is driven by an electric field, the extraction of intercalated ions can be achieved by reversing the polarity of the applied field.[97] This principle governs the mechanism of electrochromism in materials such as TMOs and MXenes.[99–101] The cations inserted into the host lattice donate charge carriers to induce a change in oxidation state, where the metal ions in the host lattice undergo a redox reaction. For instance, in WO_3, W^{6+} gains electrons to form W^{5+} and in NiO, Ni^{2+} loses electrons to form Ni^{3+}; these undergo colouration and bleaching, respectively, altering the optical absorption properties of the material.[39,99,100] This alteration of optical properties/colour change in TMOs can be due to various reasons such as the occupation of empty states by intercalated ions in the forbidden gap of the material, resulting in the formation of defect states, partial d band filling or the formation of metal complexes.[8,39,100,102–104] The ion intercalation mechanism in a TMO (such as MoO_{3-x}) is demonstrated in Fig. 2a, which depicts the bleached (OFF) and coloured (ON) states.[8] Upon application of an electric field, H^+ ions from the Nafion membrane are transferred to the MoO_{3-x} layer, resulting in the formation of molybdenum bronze ($H_y.MoO_{3-x}$). As shown in the theoretically modelled structures of self-standing and H^+

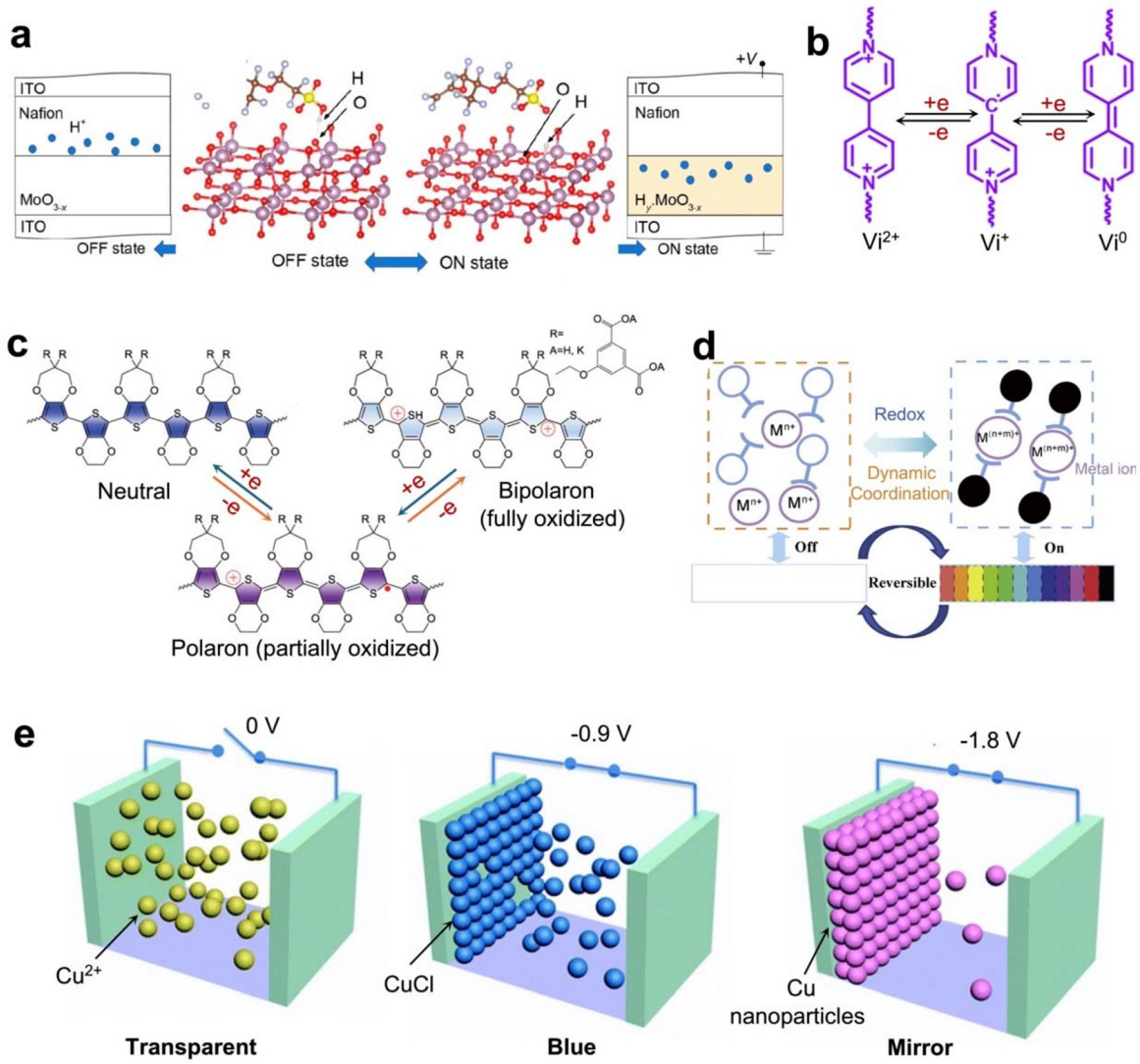

Fig. 2 Mechanisms of electrochromism. (a) Schematic illustrations of bleached (0 V) and coloured (7 V) samples upon intercalation of H^+ from Nafion ($C_9HF_{17}O_5S$) and atomic structure depictions of $C_9HF_{17}O_5S/MoO_{3-x}$ (de-intercalated) and $C_9F_{17}O_5S/H_y.MoO_{3-x}$ (intercalated). Reprinted with permission from ref. 8. Copyright 2020 American Chemical Society. (b) Molecular structure of viologen in different redox states. Reprinted with permission from ref. 105. Copyright 2020 Elsevier. (c) Schematic illustration of PPE polymer with colouration in its neutral, partially and fully oxidized states from an electrochemical redox reaction. Reprinted with permission from ref. 106. Copyright 2020 Wiley. (d) A schematic representation of the indirect electrochromic phenomenon through dynamic metal–ligand coordination and dissociation between switchable dyes and metallic ions. Reprinted with permission from ref. 107. Copyright 2021 Elsevier. (e) A schematic representation indicating the distribution of copper ions in a reversible electrodeposited electrochromic device under different biases, *i.e.* transparent state (0 V), blue state (−0.9 V) and mirror state (−1.8 V). Reprinted with permission from ref. 108. Copyright 2017 Royal Society of Chemistry.

intercalated MoO_{3-x} in Fig. 2a, the application of a high electric field helps to overcome an energy difference of 3.27 eV for ion intercalation. When this process is reversed, it results in full recovery of the Nafion molecule. In MXenes like oxygen terminated $Ti_3C_2T_x$, upon Li^+ ion intercalation, the ions are completely chemisorbed onto the MXene surface to form $Ti_3C_2T_xLi$, which modifies the material's band structure and thus the transmittance of the material.[101] This change in transmittance spectra of such MXenes through intercalation is primarily governed by the interaction between the intercalated atoms and the MXene surface.[101]

Similarly, the intercalation of K^+ ions results in an electrochemically induced colour change of a well-known metal hexacyanoferrate, *i.e.* Prussian blue.[31] Prussian blue can provide four different colouration states, *i.e.* blue, yellow, green and white. However, the yellow and green states are unstable.[109] The coloured stable state, Prussian blue, is formed from Prussian yellow by the intercalation of four K^+ ions into the interstitial sites in its unit cell, resulting in a smaller indirect bandgap.[109] This allows the compound to strongly absorb red light and reflect blue. Upon the intercalation of eight K^+ ions, the resulting Prussian blue is converted into Prussian white.[109]

This process results in the reduction of Fe ions in the metal hexacyanoferrate, which enlarges the bandgap of the material, making it transparent to visible light.[109]

3.2. Charge transfer-based redox reactions

A redox reaction involves the transfer of electrons between two different compounds and is commonly chemically induced. In viologens, alongside chemically induced redox reactions, electric field-induced redox reactions are also reported to induce electrochromic behaviour.[110] Viologens can undergo three redox reactions, as demonstrated in Fig. 2b.[105] The applied bias leads to the reduction of the ethyl viologen dication (EV^{2+}), by gaining electrons from a negative electrode and generating free radical cations (FRC), *i.e.* the ethyl viologen cation (EV^{+}), to achieve a reversible coloured state.[110] The formation of FRC results in modulation of the material's bandgap and a change in its absorbance profile.[110] For a viologen, the dicationic state (V^{2+}) is the most stable state and is colourless, whereas the radical cation is the highly coloured state (V^{+}) and the neutral state (V^{0}) is primarily pale yellow.[111] Similarly, an electrically driven redox reaction is observed in organic compounds like polymers where the application of a bias results in electron loss/gain (Fig. 2c), which is counteracted by the anions injected/extracted into/from the polymer matrix.[112] The loss of electrons results in defect-enabled energy states between the conduction band (CB) and valence band (VB) of the polymer.[112] This decreases the electronic transition energy from the VB to the CB and shifts the optical absorption of the material.[112] The loss and gain of an electron-based electrochromic colour change in electrochromic poly(3,4-propylenedioxythiophen-*alt*-3,4-ethylenedioxythiophene) copolymer (PPE) is shown in Fig. 2c.[106] In its pristine/neutral state, PPE is blue with an absorption centred around 600 nm.[106] Upon partial oxidation, it enters the polaron state with an absorption peak at ≈1000 nm; this absorption co-efficient is shifted to >1500 nm when, upon the gain of electrons, PPE is converted into a fully oxidized stable, colourless bipolaron state.[106] Hence, the electrically induced electron gain/loss based electrochromic colour change is governed by the alteration of the molecular structure of the organic compound under different redox states.

3.3. Metal–ligand interaction

Metal–ligand interaction based electrochromism is an electrically induced indirect electrochromic behaviour observed in some polymeric materials.[107] This occurs due to the coordination and dissociation of certain valence-changing metal ions and dyes upon the application of bias.[107,113] The colour change in this process occurs when metal ions generated under the influence of applied voltage form a coordination bond with molecular groups present in the system. This colour change process can be reversed by breaking the bond formed.[114] It is an unconventional process, as the application of bias regulates the valence state of the metal ions, which in turn controls the structure and colour change of the molecular switch.[115] In such compounds, the redox potential of the incorporated metal ions is lower than the oxidative potential of the polymeric compounds.[107] As shown in Fig. 2d upon the application of a bias, the metal ion valences are altered, which results in them undergoing dynamic coordination to form a coordination bond with molecular switches.[107] This results in the achievement of colouration of the molecular switches and this can be altered by the application of a reverse bias.[107] The achievement of such electrochromic behaviour is governed by the selectivity and coordination capability of the molecular switch with metal ions with special valance states, high electrochemical stability and high contrast between the bleached and coloured states.[107] The metal–ligand interaction based electrochromic phenomenon involves both organic molecular switches and inorganic metal ions and is governed by the reaction dynamics between the two.

3.4. Reversible electrodeposition

This mechanism occurs in electrodeposition-based electrochromic materials, where a simple device architecture of electrodes, electrodeposition components and electrolytes is used.[116] Upon the application of a voltage, metals dissolve in an electrolyte solution between the electrodes and deposit as films onto one of the electrode surfaces in their pristine form or in the form of an alloy, which alters the transmittance of the material.[116] Upon the application of a voltage with reverse polarity, these metals dissolve back into the electrolyte system, resulting in reversible electrochromic behaviour.[116] This is governed by the redox reaction of a metal in the electrolyte and has been demonstrated using different metals such as Ag, Bi, and other cations.[116,117] Reversible electrodeposition-based electrochromism is demonstrated in Fig. 2e.[108] In their transparent state, Cu^{2+} ions are randomly distributed in a gel electrolyte between ITO electrodes.[108] The application of −0.9 V results in the formation of a greyish blue film of CuCl.[108] However, when a higher potential (−1.8 V) is applied, it results in the conversion of Cu^{2+} into Cu^{0}, which is deposited onto the electrode, resulting in a mirrored state.[108] The application of a positive potential results in the reversal of the process and the dissolution of Cu back into the electrolyte.[108] Thus, reversible electrodeposition is governed by electrically induced formation and dissolution of metallic or metallic compound based films on an electrode that alter the transmittance of the device, enabling a colour change.

In summary, ion intercalation-based electrochromism, as seen in transition metal oxides, offers advantages like high coloration efficiency, long-term stability, and low operating voltages. However, electrochromism generated in this way can suffer from slow switching times due to the diffusion-controlled ion transport process and slower life cycle due to the acid. Charge transfer-based redox reactions, observed in organic materials like viologens and conjugated polymers, enable multiple colour states, rapid switching speeds, and tunable optical properties. Nonetheless, these materials often exhibit limited stability and require encapsulation.

Metal–ligand interactions in coordination complexes provide a unique opportunity for fine-tuning the electrochro-

mic properties through ligand design. However, these complexes can be susceptible to degradation and may require careful electrolyte selection. Reversible electrodeposition offers advantages like high coloration contrast, but it can be challenging to achieve uniform deposition and prevent material dissolution over prolonged cycling.

Ultimately, the choice of electrochromic mechanism depends on specific application requirements. Ion intercalation and reversible electrodeposition are well-suited to applications demanding high durability and coloration contrast, like smart windows. Charge transfer-based redox reactions and metal–ligand interactions are more suitable for applications requiring rapid switching and tunable optical properties, such as displays and optoelectronic devices. Strategies like compositing and nanostructuring can be employed to mitigate the limitations associated with each mechanism.

Density functional theory (DFT) methods are particularly valuable to study electrochromic processes accurately at the atomic level, especially in calculating and analysing properties that are challenging to obtain experimentally. The insights gained from DFT calculations not only explain the material properties but also facilitate the rational design of new molecules with specific electrochromic properties.[118–122] The intercalation effect of different metal cations, such as Li^+, Zn^{2+} and Al^{3+}, on the electrochromic properties of different materials is studied by DFT models.[119,120]

One key area of progress is the intersection of AI-driven electrochromic materials and nanofabrication processes, particularly in machine learning (ML)-integrated environments.[123] Significant improvements to the device design (single and dual flexible ECDs), production, and performance optimization can be made with a combination of AI and EC materials.[124–126] AI helps in the optimization of the material's properties by analyzing large datasets and complex algorithms, which reduces the need for time-consuming empirical trials. Several groups like Tällberg *et al.*[127] and Khatibi *et al.*[128] have developed algorithms to manage the transparency of smart electrochromic windows (SEWs), with results showing significant energy savings of up to 40–65% in different locations. Although ML has been successfully applied in areas like light emitting diodes (LEDs), quantum dot LEDs (QLEDs), and solar cells, its use in electrochromics has been limited.[125] Some research has utilized ML techniques to predict and optimize electrochromic device performance, but a comprehensive evaluation method that integrates multiple performance indicators is still lacking. This is an area where untapped opportunities exist for the research community to investigate the potential of ML and AI in a more targeted manner.

4. Electrochromic degradation prevention and reversal strategies

While considering real world applications, device lifetime is one of the crucial factors for cost-efficient sustainable technology. Like every other material, electrochromic materials also suffer from degradation over prolonged use. Hence, strategies to counteract rapid deterioration or return the said material to its initial state are important for recycling and prolonging device lifetimes. This section discusses strategies to prevent ion trapping in materials arising from ion intercalation and extract trapped ions from host lattices and a convenient method to reduce degradation dynamics of PB to fully exploit their superlative electrochromic properties.

For electrochromic colouration of metal oxides, monovalent metal ions such as hydrogen ions (H^+), lithium ions (Li^+) and sodium ions (Na^+) are widely used for intercalation purposes due to their property of a low diffusion energy barrier, thereby, improving their switching time and high charge density, enabling a high CE.[129] However, despite this advantage, the usage of monovalent ions alone can result in durability problems. For instance, H^+ ions can be corrosive due to their acidic nature, Na^+ can cause excessive lattice expansion due to its large ionic radius and Li^+ can be reactive under ambient conditions.[25,129,130]

In contrast, the use of multivalent ions like zinc (Zn^{2+}), magnesium (Mg^{2+}) and aluminium (Al^{3+}) seems to eradicate these concerns. Firstly, less cation involvement in the process of intercalation/deintercalation provides multivalent ions with improved stability. Additionally, despite their low mobility, multivalent ions can provide increased charges for intercalation compared to their monovalent counterparts. They are also cost-efficient, safe and highly compatible with aqueous electrolytes.[131] As such, multivalent ions have been employed in several electrochromic materials and devices such as those that have been successfully implemented in various applications.[25,129–131] As reported by Yao *et al.*, the use of Al^{3+} as an electrolyte instead of Li^+ allowed for multi-electron redox reactions.[25] Also a comparison of quantum dots (QDs) in Li^+ and Al^{3+} electrolytes showed enhanced stability in the latter.[25] This can be attributed to the smaller ionic radius of Al^{3+} causing less lattice expansion of the host material during the ion insertion/extraction process.[25]

Another challenge with ion intercalation in metal oxides is the degradation of electrochromic performance and performance stability as a result of ions trapped in the host material due to electrochemical cycling.[132] This occurs because the host electrochromic material consists of both shallow intercalation sites with low energy barriers (that enable fast ion diffusion/reverse diffusion) and trap sites with high energy barriers (which immobilize diffused ions).[133] Such trapped ions can be de-trapped when they are provided with a high energy supply to overcome the energy barrier in the trapped state.[102] Studies have reported the application of potentiostatic and galvanostatic mechanisms for Li^+ ion de-trapping to revert the degraded electrochromic films to their original state and performance.[132,133] Similarly, Sorar *et al.* reported the use of a potentiostatic rejuvenation mechanism for W–Ti oxide thin films.[134] Here, the films were subjected to a constant 6 V bias for 20 h for ion de-trapping followed by a 2 h resting period after 200–300 cycles of electrochromic efficiency loss.[134]

Following potentiostatic treatment, the films recovered their original electrochemical cycling efficiency.[134]

Even though these strategies have proved to be effective for the above-outlined electrochromic bulk films, it is felt that there is an absolute need to formulate other strategies that result in improved performance. Modulation techniques such as nanostructuring, porosity induction and compositing can improve the lifecycle of electrochromic materials, as outlined in the next section.

5. Modulating electrochromic properties

With an ever-increasing need for improved performance in smart devices and extended lifecycles along with economical production, there is a need to further engineer a material's innate electrochromic properties. This section analyses various strategies such as nanostructuring, doping, compositing and other strategies that have been used to modulate the electrochromic performances of materials.

5.1. Nanostructuring

Nanostructuring provides an exciting pathway to not only tune but enhance the electrochromic performance of materials. Nanostructures have gained a lot of attention in the past decade due to their distinct material and functional properties in comparison with their bulk counterparts. For example, low dimensional structures alleviate problems associated with extended ion traversing lengths and restricted ion diffusion in flat films that affect the electrochromic switching time and optical contrast in a material.[5] Studies have reported that strategies that introduce porosity into deposited films or nanostructures enable shorter ion diffusion pathways, and faster ion diffusion due to improved contact with the electrolyte.[1,16] In addition, it also reduces the oxidation and reduction potential of the materials occurring from a lower contact resistance between the nanostructure and the electrolyte.[16,135] This facilitates an overall reduction in energy consumption of the system.[16] Moreover, a high surface-to-volume ratio in nanostructures provides an increased number of ion intercalation sites.[4,5,8,18] The following subsections entail a detailed discussion of the various nanostructuring mechanisms that can be considered to modulate electrochromic properties.

5.1.1. Two-dimensional nanostructures. The presence of inter-layer spacing in the layered two-dimensional (2D) nanostructures creates penetrable channels and high specific areas that provide comprehensive material–electrolyte contact[136] and enable higher ion diffusion.[136] Such structures are comprised of exposed surfaces, thereby, providing opulent atoms to facilitate surface/interfacial electrochemical reactions.[137] The ability to alleviate substrate contact issues, which are often unaddressed in one-dimensional (1D) nanostructures or three-dimensional (3D) mesoporous morphology for better bending performance on flexible substrates, makes 2D nanostructures more attractive for this field of study.[138] As such, 2D TMOs and their heterostructures provide an exciting avenue for tuning electrochromic properties.[8,18,43,136,138–141] Li *et al.* demonstrated a 2D TiO_2/MXene ($Ti_3C_2T_x$) heterostructure for a flexible EC device, as shown in Fig. 3a [142] where the TiO_2 film served as an EC layer and the $Ti_3C_2T_x$ layer acted as a transparent electrode.[142] The use of a $Ti_3C_2T_x$ layer as a counter electrode can enable efficient electron transport between the EC layer and the counter electrode due to the low work function of $Ti_3C_2T_x$ in comparison with conventional ITO electrodes.[142] The film exhibits higher colouration with increasing thickness of the TiO_2 layers due to higher optical modulation.[142] Fig. 3b denotes the CE of EC films comprising one, four and seven layers of TiO_2. The highest CE is observed for the single variant without much deterioration with an increasing number of layers.[142] The high CE is due to efficient charge insertion/extraction, resulting in a much higher CE in comparison with bulk-dense TMO films.[142] Furthermore, as seen from Fig. 3c, the colouration and bleaching times of the TMO layers are significantly shorter and comparable to that of organic electrochromic films. This can be attributed to the efficient ion diffusion process in a 2D structure, as shown in Fig. 3d, where the redox reaction takes place throughout the entirety of the film rather than being restricted to the surface. Similar performance improvements have been observed in 2D nanostructures of both WO_3 and MoO_3 in comparison with their bulk counterparts; this can be attributed to the penetrable channels from the 2D morphology, which provide more intercalation sites and shorter diffusion lengths.[18,43,143] Arash *et al.* developed a non-stoichiometric oxygen-deficient MoO_3 2D nanosheet-based, spectrally selective electrochromic device.[8] The device demonstrated a high colouration efficiency of 116 $cm^2\ C^{-1}$ at 392 nm; this is attributed to improved ion intercalation occurring in the van der Waals gap due to the material's high surface-to-volume ratio.[8]

Similar to their inorganic counterparts, 2D polymeric nanostructures provide benefits such as distinct charge transport in comparison with 1D structures due to their large in-plane p-conjugated backbone and π–π stacking.[145,146] The improved charge transportation in the afore-mentioned structure has been used to develop co-ordination nanosheets (CONASHs) and covalent organic framework (COF) nanosheets for electrochromic devices.[145,146] The electrochromic properties of a CONASH usually depend on the structure of its organic ligands and the metal ions.[145] A ferrous ion (Fe^{2+}) based 2D metal coordination complex with bis(2,2′-bipyridine) based ligands reported by Bera *et al.* exhibited a CE of 431 $cm^2\ C^{-1}$ at l = 590 nm with sub-second colouring and bleaching times,[147] indicating a lower power requirement for colouration and improved ion diffusion. Such performance is rarely seen in 1D and 3D coordination polymers. Similarly, a Fe^{2+} based nanosheet with tris(1,10-phenanthroline) ligands was used to construct an EC device with stability over 15 000 cycles[145] but with a lower CE than that of the complex with bipyridine ligands.[147] The reported high cycling stability of the Fe^{2+} based nanosheet with tris(1,10-phenanthroline) ligands is much higher than that of other reported 2D CONASHs, which range

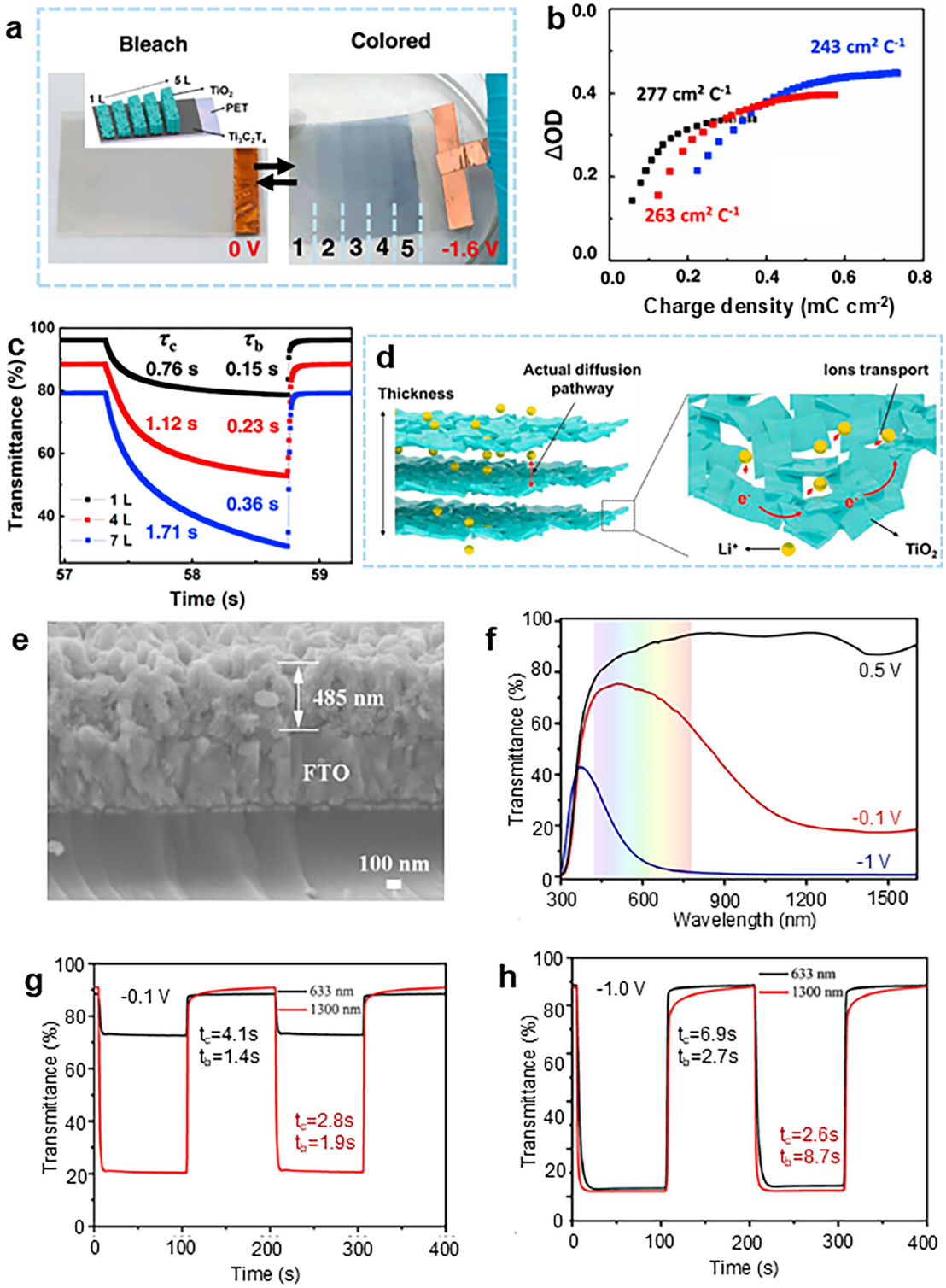

Fig. 3 Structuring mechanisms to modulate EC performance. (a) Photograph of a 2D $TiO_2/Ti_2C_3T_x$ heterostructure under bleached (0 V) and coloured (+1.6 V) conditions with a different number of layers of TiO_2 (1–5 layers). (b) Charge density based on injected charge indicating the CE of 1L, 4L and 7L $TiO_2/Ti_3C_2T_x$ heterostructures. (c) The temporal response of colouration and bleaching for different thicknesses of TiO_2 layers in the heterostructured EC devices. (d) 3D schematic of the intercalation mechanism and electron conduction for electrochromism in TiO_2 films. Reprinted with permission from ref. 142. Copyright 2021 Springer Nature. (e) Cross-sectional SEM image demonstrating the porous morphology of the WO_3 nanowires and nanoparticle film. (f) Optical transmittance spectra of WO_3 nanowires and nanoparticle film under different voltages in a 1 M $LiClO_4$/PC electrolyte. Transmittance spectra modulation of the film in the electrolyte under square wave potential at (g) 0.5 V and −0.1 V (h) 0.5 V and −1 V at 633 nm. Reprinted with permission from ref. 144. Copyright American Chemical Society.

from 300 to 500 cycles.[145,147–150] As these 2D CONASH properties are inherently dependent on the metal centres and organic ligands, the desired physiochemical properties can be achieved by regulating their molecular composition.[147] Such nanosheets, when fabricated using a bottom-up approach, provide control over the structure of the sheets and can be fabricated at a low cost.[147,151] The presence of an oriented porous structure and π–π stacking of 2D COFs provide a great opportunity for integrating them into electrochromic devices.[146] Despite their high CE and rapid switching kinetics, these materials have been understudied for their electrochromic properties.[146,152] A further study into different complex formations can provide a pathway to improved EC performances from one single CONASH structure. An analysis of the current literature indicates a trend of highly efficient intercalation in 2D morphologies resulting in a reduced switching time and enhanced colouration efficiencies due to their atomically thin nature and large exposed surface areas. Moreover, for facile synthesis techniques, these nanosheets can often be dispersed in solution and deposited using inkjet printing and spray coating techniques, for large-scale production.[43] This can be a pathway to highly efficient low-cost electrochromic technology. Despite these advantages 2D nanosheets often suffer from restacking, which can limit their free surface energy due to aggregation, hindering effective ion intercalation.[140] This issue can possibly be addressed by strategies to prevent the restacking of 2D sheets.[153,154]

5.1.2. 1D nanostructuring. Similar to 2D nanostructures, 1D nanoarrays such as nanotubes, nanoribbons and nanowires provide innumerable advantages, some of which are faster and directional ion transport, reduced intercalation induced stress from lower rigidity at high aspect ratios, higher optical modulation, and improved contact between the materials and electrolyte occurring from their high surface areas.[155–157] Additionally, 1D nanostructures consist of inter-structure spacing that prevents cracking of the material by alleviating strain occurring as a result of volume expansion from intercalation.[4,157,158]

Researchers have widely employed 1D nanostructures such as nanorods,[4,159] nanowires,[160,161] nanopetals,[162] nanotubes[163] nanobelts,[164] and nanoneedles[68] to engineer electrochromic properties. For instance, PB nanostructures based on 1D TiO_2 nanorods have shown better electrochromic performance and stability compared to PB films.[4,11] 1D nanostructured PB helps to reduce the lattice stress occurring from volume expansion during ion intercalation and also enables better substrate adhesion due to increased surface roughness along with reduced ion diffusion length and higher ion storage sites.[4,11] In a study by Zhao *et al.* the realisation of PB on WO_3 nanorods results in improved stability of the material by alleviating lattice expansion stress.[165] Furthermore, the heterostructure of two different materials resulted in efficient electron transfer.[165] Thus, nano-structuring often addresses the issues of poor substrate adhesion affecting PB thin films.[4,165] Similarly, PEDOT placed on TiO_2 nanorods resulted in a significant improvement to the electrochromic efficiency and cycling stability in comparison with the same material in film form.[166] Furthermore, the nanorod architecture has also been utilised to model other inorganic materials such as V_2O_5, WO_3 and niobium pentoxide (Nb_2O_5) for modulating their electrochromic properties.[157,159,167] Bulk films of V_2O_5 have shown a slower electrochromic performance and lower optical contrast, which arises from its low electrical and ion conductivity.[167] This limitation can be overcome by nanostructuring to increase the surface area and conductivity.[167]

Other structures such as nanorods and nanowires have been implemented to construct 1D organic EC devices with improved CE, optical modulation and response times.[158,160,161,168] While a poly(indole-6-carboxylic acid) (PICA) film exhibited a CE of 102 $cm^2\ C^{-1}$, a PICA nanowire array had a high CE of 142 $cm^2\ C^{-1}$ at 490 nm due to the 1D morphology enabling better charge transfer at the surface and within the material.[158] As reported by Li *et al.* the nanowires resulted in a shorter ion diffusion path, and hence, faster switching speed.[158] Despite their much revered benefits, 1D nanostructure arrays often involve a two-step complex fabrication process, which can be costly and time consuming.[169] Therefore, simplified synthesis techniques would be beneficial for enabling commercial application based on 1D nanostructures.

5.1.3. Zero-dimensional nanostructuring. The ultimate size confinement of zero-dimensional (0D) QDs makes way for speedy charge transfer through the interface and within the material.[25] The presence of a large number of surface atoms in such structures results in higher electrochemical reaction rates.[63] Similarly to other nanostructures, they exhibit shortened ion pathways from improved surface-to-volume ratios.[63] Moreover, the size quantization of QDs below their exciton Bohr radius can result in strong quantum confinement along with the small size greatly shortening the diffusion path of ions.[63] Below are some of the exemplary performances shown by 0D-based EC devices.

Typically, TMO-based QD nanoparticles have been explored immensely for EC applications.[25,170] Yao *et al.* reported the use of a cost-effective atmospheric pressure solution-based deposition (APSD) method for fabricating WO_3 QDs with significantly improved cycling stability (20 000 cycles).[25] A comparison between WO_3 QDs synthesized by Yongji *et al.*[25] and Cong *et al.*[63] shows that the high stability of the former is due to the absence of organic encapsulation and the use of multivalent electrolytes.[25] The presence of a hydrophilic organic aliphatic amine enhanced the electrolyte permeation into the QDs resulting in a higher CE of 154 $cm^2\ C^{-1}$ at 633 nm.[63] However, the water solvency of organic encapsulation alongside the corrosive nature of the H^+ ion based electrolyte caused the QDs to peel off, resulting in a low stability of 50 cycles.[25,63] Recently, transition metal dichalcogenide QDs based on molybdenum disulphide (MoS_2) were also used in ECDs.[171]

A comparative study between QDs, flakes and bulk materials revealed that the QD based ECD outperformed the rest due to improved charge penetration into the host lattice occurring from the 0D morphology.[171] Despite readily available

facile synthesis techniques,[25,172] EC QD structures with diameters less than 5 nm are sparsely reported in the literature due to the complexity associated with the fabrication processes, particularly reduced product yields.[172] Also QDs can result in a higher number of grain boundaries in the film, hindering charge transfer.[173]

5.1.4. Plasmonic nanostructuring. Plasmonic nanostructures manipulate light at the nanoscale and can be applied to electrochromic devices to tune the contrast for a stark colouration effect.[174–176] A key advantage of these structures is that they provide spatial confinement, which is associated with surface plasmon polariton (SPP) electromagnetic radiation that enables the operation of these devices beyond the optical diffraction limit.[175,176] They also enable the generation of vibrant colours due to intrinsic resonance through interactions with light.[176,177] The introduction of plasmonic metasurfaces into WO_3 and dimethylpropylenedioxythiophene ($PProDOTMe_2$) resulted in an approximately 25–35% enhanced brightness over commercially available electrophoretic displays.[174] Similarly, the interaction of confined light with the WO_3 based electrochromic optical cavity resulted in high-contrast electrochromic red, green and blue colouration of pixels for different film thicknesses of 170, 235, and 210 nm, respectively.[178] Various plasmonic metasurfaces such as nanoslits,[175] nanowells[179] and nanoparticles on a mirror[180] have been employed to construct polymer based electrophoretic displays. Despite their ability to produce stark colouration with high switching speeds, the commercialization of plasmonic devices is often hindered by the scalability and complexity of fabrication processes.[180] However, nanoimprint lithography associated with procuring high-resolution patterns can often enable the cost-efficient production of large scale photonic devices.[181] Peng *et al.* reported the fabrication of lithography free polymer based electrochromic nanoparticles on a mirror (eNPoM) based nanopixels with improved switching contrast resulting from the plasmonic nanostructures.[180] The eNPoM structure enables fast electron transfer between PANI and the gold (Au) mirror with millisecond range switching speeds, which are critical in the development of fast displays with lower energy consumption.[180] Similarly, a 25 nm PANI film on an Au nanoslit offered a switching speed of 9 ms (ref. 175), which was faster than industrially producible electrophoretic displays with an approximately 1 s switching speed[174] and comparable to liquid crystal displays (LCDs) with switching speeds of around 20 ms.[182]

5.2. Three-dimensional porous structures

Due to small pore dimensions (2–50 nm), 3D mesoporous thin films have high porosity.[5] This translates to a higher density of intercalation sites and improved surface to volume ratios, thereby enhancing the CEs. Mesoporosity based nanostructures have been utilized for an array of high efficiency electrochromic organic and inorganic materials.[5,183–185] Zhang *et al.* reported a unique honeycomb-like nanostructured PANI-based electrochromic film.[44] Relatively higher optical modulation (700 nm) of 62.4% was observed in nanostructured PANI films compared to 26.1% in bulk PANI films. This is because intercalation in bulk films is limited to the material surface, due to high film density.[44] The presence of porosity in films further results in reduced charge transfer resistance enabling faster ion diffusion with a quicker response time and reduced oxidation voltages.[44] The porous film also had a high CE of 216.3 $cm^2\ C^{-1}$, which indicated greater optical contrast at reduced power.[44] Effective charge transfer resulting in a millisecond range response time was also possible with a gyroid-structured 3D V_2O_5 film, which had highly periodic interconnected structures with smaller pore diameters.[5] The overall optical modulation and switching times of microporous films (pore diameters > 400 nm) were inferior to those of the mesoporous V_2O_5 films (pore diameters between 2 and 50 nm).[5] Similarly, the introduction of mesopores into Ni-metal oxide framework (MOF) films resulted in relatively high stability for 20 000 cycles, which could be attributed to the mesopores reducing the stress of volume expansion upon intercalation.[1] In a study by Liu *et al.*, the use of WO_3 nanowires and nanoparticles in a film form resulted in the formation of a porous architecture, as shown in the cross-sectional SEM of the film in Fig. 3e.[144] The porous structure demonstrates selective modulation in the visible and NIR regions based on the applied bias, as seen in Fig. 3f, which can be attributed to the localized surface plasmon resonance (LSPR) effect in some nanoparticles.[144] The film demonstrates a much higher switching speed for modulation in both the visible and NIR domains, as shown in Fig. 3g and h; this is higher than other reported dual-band electrochromic devices.[144] This can be attributed to the presence of pores in the film that allow for the easy transfer of Li^+ ions into the film for efficient intercalation.[144] One of the key advantages of such porous structures is easy reproducibility using simple techniques such as chemical bath deposition (CBD) and electrodeposition.[183,184] One of the key requirements of such structures is a uniform interconnected network with a narrow pore diameter distribution for effective electrolyte contact.[5] Also, for rapid response speeds, the strut radius of the film should be similar to the ion diffusion distance and a reduction in feature size can often lead to reduced stability and lower conductivity.[5] Despite the advantages of mesoporous networks, the formation of such architectures is often associated with multi-step processes.[1,5,44]

5.3. Doping

Doping has been reported to improve structural/electrical properties, increasing ion diffusion, durable electrochromic performance, colouration efficiency, optical modulation and cycling stability of different materials for energy-saving technologies.[186,187] For instance, the EC properties of materials like NiO and WO_3 are improved by Ti doping, which reduces lithium-ion capture sites, or Ag, which improves conductivity and charge transfer resistance, although the response time remains a challenge.[188–190] As Kumar *et al.* reported, MoO_3 films doped with different concentrations of W showed improved CE, reversibility and cycling stability compared to

the pure MoO_3 films.[10] Doping MoO_3 with W causes changes to the film's microstructural properties, which govern the mobility of intercalating Li^+ ions.[10] The increased crystallite size upon doping improves the surface area of the films.[172] The improvement in the surface area is associated with facilitated electrochromic reaction kinetics. Studies on doped WO_3 have reported improved performances that could be attributed to increased carrier density, charge transportation properties and conductivity.[191,192] The improved conductivity arises from the exchange of electrons between the host and dopant atoms.[193] Moreover, non-stoichiometric oxides doped with oxygen ionic conductivity can introduce oxygen vacancies to improve the ionic conductivity of the oxide.[194] N doping resulted in improved electronic conductivity for improved charge transfer in NiO whereas doping WO_3 with Ti enabled an increased surface area of WO_3 resulting in superior electrochromic colouration in comparison with undoped WO_3.[140,172] As reported by Zhan *et al.*, the introduction of Ti dopant reduced the crystallite size of WO_3 to improve its active surface area, so more WO_3 would be available for ion intercalation.[172] However, it is reported that low Ti-doped WO_3 films perform better in electrochromic tasks due to a star-like crystallite structure that reduces resistance to charge transfer and ion diffusion. This boosts their electrical conductivity and reaction speed.[195]

The introduction of Ti dopant, as shown by Zhan and co-workers, resulted in low ion diffusivity from reduced lattice spacing in WO_3.[172] Similarly, in a study by Hou *et al.*, doping NiO with 10% by weight of tin (Sn) resulted in an improved electrochromic performance and a reduction in film thickness.[196] This is due to the reduction in surface energy of NiO through Sn doping, which prevents stacking of the nanosheets and increased porosity of the film.[196] Thus, doping enables faster bleaching and colouring times of 0.4 s and 3 s in the doped film in comparison with the undoped one, as shown in Fig. 4a and b, respectively.[196] Other doping strategies such as co-doping lithium (Li) along with other materials such as Ta, Zr, Cu and Mg often enable a change in the material's surface morphology for an electrochromic reaction.[199,200] This technique has been widely applied to enhance the electrochromic performances of NiO films,[199,200] resulting in improved electrochromic responses.[201,202] However, with doping strategies, achieving the correct concentration is key to optimising performance, as higher doping concentrations can lead to performance degradation.[10,135]

5.4. Composite materials

Similar to doping, composite structuring has also been shown to tune electrochromic properties. Composite structures are mostly comprised of organic/inorganic, inorganic/inorganic or organic/organic material combinations, which utilise the electrochromic properties of both components. Compositing inorganic and organic materials for enhanced electrochromic performance has been widely deployed for electrochromic devices.[17,75,203,204] The presence of properties from both organic and inorganic components in inorganic–organic composite materials enables them to display higher colouration efficiencies due to the synergistic colouration of individual materials[205] and better cycling stability.[17] It is well known that, despite having stark colouration and better switching speeds in comparison with TMOs, organic polymers often undergo irreversible degradation from intercalation stress.[17] Hence, several studies have adopted the strategy of compositing inorganic materials and organic conducting polymers (CPs) for improved electrochromic performance.[206–208] The use of TMOs in conjunction with CPs often leads to the formation of a porous morphology for better ion transport, resulting in a donor–acceptor mechanism for improved stability and improved electron transport due to their complementary conduction.[75] In a study by Guo and co-workers, the utilization of p-type polyindole with n-type WO_3 resulted in a donor–acceptor approach from the strong ionic bonds between nitrogen and tungsten atoms.[17] This resulted in improved ion diffusion and facilitated electron transport.[17] Also, the film had a high cycling stability from the strong adhesion of WO_3 to the substrate and the porous morphology, which reduced stress on the material during the redox process.[17] Composite materials can help engineer dual band electrochromism enabled by different spectro-electrochemistry of the individual components.[209] A complementary indium tin oxide (ITO):PANI nanocomposite based electrochromic material developed by Yilmaz *et al.* showed optical modulation in the visible and infrared regions of the spectrum, resulting from the individual spectral responses of each material.[209] A high CE of 293 cm^2 C^{-1} at 1600 nm and 228 cm^2 C^{-1} at 600 nm was obtained along with a high optical modulation due to a fast charge transport mechanism and high contact area occurring from the strong chemical bond between the complementary materials.[209] Similarly composites of organic viologens and inorganic materials have resulted in dual band electrochromism.[203] The presence of complementary switching mechanisms between the inorganic and organic components of the composite resulted in superior charge transfer resulting in the viologen switching quickly at a lower bias.[203,204] In another study by Mohanadas *et al.*[197] an inorganic/organic composite film was demonstrated to improve the CE and optical modulation of the Cu based MOF and WO_3 composite in comparison with the individual components, as shown in Fig. 4c.[197] Despite the porous nature of the MOF, its poor electrical conductivity results in a low EC performance.[197] This is improved by the addition of electrochemically conductive WO_3 to the MOF. Thus, a higher CE of 296.4 cm^2 C^{-1} is observed in the composite, which is higher than that of WO_3 itself (85.3 cm^2 C^{-1}) and can be attributed to the short diffusion pathway in the composite structure.[197] Hence, it can be seen that inorganic/organic composites can show dual band electrochromic properties, altered film morphology and improved electrochemical activity, demonstrating multiple colouration states and improved electrochromic efficiency. Also, the complementary switching mechanism can result in fast charge transfer, enabling rapid-switching electrochromic devices. Moreover, organic/inorganic composites often extend the lifecycle of polymeric films.[210]

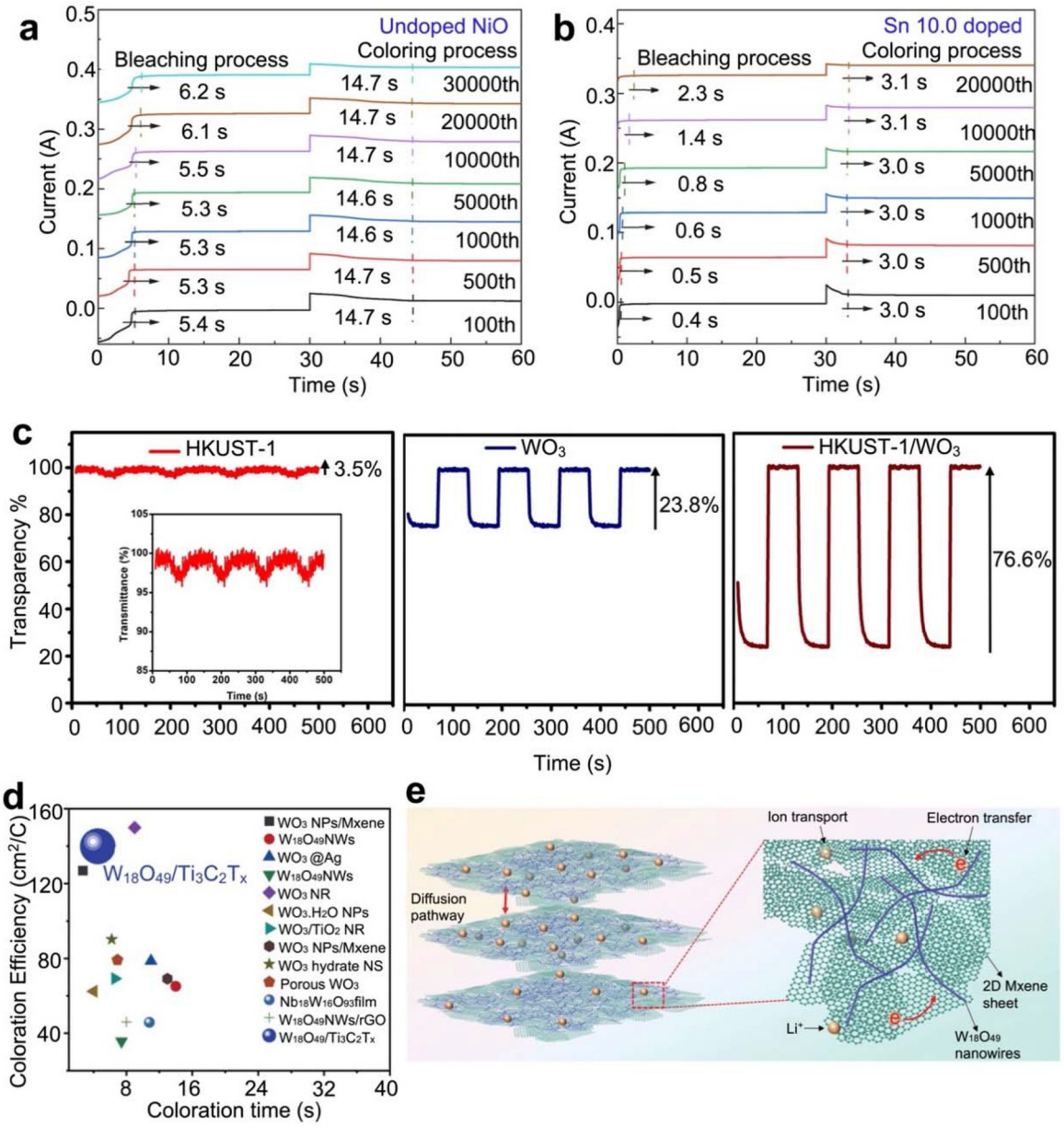

Fig. 4 Doping and compositing mechanisms to modulate EC performance. Colouring and bleaching of (a) undoped NiO and (b) NiO doped with 10% Sn. Reprinted with permission from ref. 196. Copyright 2023 Elsevier. (c) A comparison of transmittance modulation of HKUST polymer, WO_3 and the composite of HKUST and WO_3 at 633 nm. Reprinted with permission from ref. 197. Copyright 2022 Elsevier. (d) Colouration efficiency and colouration time comparison of $W_{18}O_{49}$ nanowires and $Ti_3C_2T_x$ composite film with other $W_{18}O_{49}$ composites and standalone films. (e) A 3D schematic representation of ion diffusion and electron conduction for electrochromism in the aforementioned composite film. Reprinted with permission from ref. 198. Copyright 2024 Wiley.

Several studies have reported the use of various transition metal oxides to form composite systems for enhanced electrochromism.[7,9,211,212] The use of other metal oxides in conjunction with WO_3 enables improved electrical conductivity due to the interaction of the host and the dopant, as well as the inhibition of cluster formation during deposition.[213] Jittiarporn *et al.* reported an inorganic WO_3:MoO_3 composite film with improved electrochromic performance in comparison with its pure WO_3 counterpart.[9] This can be attributed to the presence of defect states in the composite film resulting in a higher ion storage capacity.[9] The addition of MoO_3 also increased the surface roughness of the film, enabling greater ion diffusion due to an improved surface area and better electrochromic performance.[9] A cost effective electrochemical deposition method for the fabrication of composite niobium pentoxide (Nb_2O_5) and tantalum pentoxide (Ta_2O_5) was reported by Saez Cabezas *et al.*; this provided scalable fast growth rates under atmospheric conditions.[214] Nam and co-workers

composited iridium oxide (IrO_2) with gold nanoparticles, and revealed that such a hybridization eliminated slow electron migration between the oxide metal interface of a conventional electrochromic device and thereby showed faster switching kinetics.[215] Despite their enhanced performance, inorganic hybrids often lack the multiple colouration/dual band electrochromic properties that can be obtained from organic hybrid materials.

Polymeric materials are attractive for real world applications by using the changing cross-link density strategy to effectively improve the stability, optical contrast and colouring efficiency.[95,216] For example, Chandrasekhar *et al.*[95] reported several new monomer precursors of cathodically colored conducting polymers for electrochromic lenses with high contrast (up to 70%/7% transmission), durability (>10 000 cycles), and fast switching times (<1 s), which have been successfully integrated into practical, safety-standard compliant smart glasses. Organic viologens, on the other hand, show that their comproportionating reaction of V^{2+} and V^0 states, dimerization, recrystallization and aggregation on electrodes degrade the device performance, despite their high optical modulation in the visible regime.[217,218] Hence, researchers have employed strategies to combine viologens and polymers as electrochromic materials and electrolytes, as well as composite them for stark multicolour electrochromism to achieve stability enhancement.[105,218–220] For instance, the use of a polymeric matrix in a viologen based electrochromic device as an electrolytic gel enables the electrostatic attraction of viologen ions,[217,218] which prevents aggregation and a reduction in the diffusion rate of viologens; this is highly beneficial for long term stability.[217,218] As shown by Wu and co-workers, the use of a polymer matrix as an electrolyte gel resulted in the viologen based device retaining 91.3% of its initial optical modulation after 10 000 cycles.[218] This improved cycling stability resulted from the presence of fluorine in the polymer matrix, which attracted viologens due to their negative charge, thereby preventing their aggregation.[218] Similarly, in a study by Liu *et al.* heptyl viologen (HV) was used as a gel electrolyte for a polymer based electrochromic system.[219] The use of long HV chains in the electrolyte resulted in steric hindrance, which prevented the agglomeration of viologens and resulted in improved stability.[219] The anodic polyamides and cathodic HV acted as complementary charge storage layers, where HV acted as a charge trapping layer and greatly reduced the bias required for the system.[219] Other than improved stability and enhanced electrochromic performance, organic composites often result in multiple colouration[220] states and lower reaction potentials.[219] As shown by Zhou *et al.*, the use of a viologen and polymer composite resulted in the formation of four redox peaks occurring from the two negative potential peaks of viologen and two positive potential peaks of the polymer (oligoaniline).[220] Viologens act as electron transfer mediators for the oligoaniline redox reaction and oligoaniline acts similarly during the viologen redox process, which in turn can potentially reduce the switching voltages between the intermediate states.[220] The utilization of viologens and a polymer matrix results in colouration arising from the negative potential of viologens and the positive potential of the polymer matrix, enabling multiple colouration states in the same material.[105] Moreover, the use of organic composites/hybrids can often result in truly transparent to black electrochromism, which can be vital for electrochromic displays.[219] As shown by Liu *et al.* the use of HV in conjunction with electroactive polyamides (PAs) with *N*,*N*,*N*′,*N*′-tetraphenyl-*p*-phenylenediamine (TPPA) and tetraphenylbenzidine (TPB) units resulted in transparent to black electrochromism.[219] The truly black state was enabled by the convergence of the three primary colours, red, blue and green, originating from the individual electrochromic materials. The black colouration improved as the thickness of the film increased,[219] which could be an issue for fast ion diffusion. The resulting film had a longer colouration/bleaching time in comparison with other polymeric ECDs.[44,219]

Both nanostructuring and composite materials provide pathways for modulating the electrochromic properties of materials. Various studies have selectively combined both these strategies to precisely engineer electrochromic materials and devices with desired properties.[15,155,221] Multiple investigations have utilized compositing strategies to obtain synergistic electrochromic material properties arising from inherent properties of their individual components, along with nanostructuring for faster charge transfer kinetics and reduced charge injection for colouration.[15,16,155,221] Studies have implemented this approach to obtain nanostructured inorganic–inorganic[15,137,215] organic–organic[16,222] and organic–inorganic hybrids[155,221,223] that exhibit high optical modulation, show multiple colouration states, possess better cycling stability and prevent degradation from the electrolytic medium, and can exploit different functionalities in a single device. In a study by Tang *et al.*, a nanostructured composite, WO_3:V_2O_5, resulted in a high current density from nanostructuring and rarely observed multiple colouration states in inorganic materials due to the presence of complementary electrochemical activity from both WO_3 and V_2O_5.[15] An ITO nanocrystal embedded with amorphous Nb_2O_5 showed not only the unique properties of the individual materials but also superior properties in comparison with those of the individual amorphous oxide and had a high cycling stability (2000 cycles).[224] The nanostructured composite transforms from a transmissive state to NIR blocking and visible light blocking states under different biases due to the presence of ITO and Nb_2O_5, respectively.[224] In a recent study, Hassan *et al.* reported a composite film of $W_{18}O_{49}$ nanowires and $Ti_3C_2T_x$ MXene designed to alleviate limited conductivity and low ion diffusivity issues faced by electrochromic tungsten oxide films.[198] The film shows improved CE and colouration times in comparison with other reported WO_3 films and composites, as shown in Fig. 4d.[198] This is due to improved charge insertion and extraction in the composite film and the dual underlying phenomena, as demonstrated in the schematic in Fig. 4e.[198] Firstly, the use of a 2D MXene allows for efficient Li^+ ion diffusion in the nanochannels due to highly exposed surfaces from the 2D and 1D morphology in comparison with pure $W_{18}O_{49}$ nanowire

films.[198] Secondly, the composite film shows a near-metallic electronic conductivity, promoting efficient electrochemical activity within each layer, resulting in improved EC performance.[198] As such, it appears that a combination of nanostructuring and hybridisation approaches may harbour untapped potential for high-performance electrochromic materials.

6. Applications

The visible change in colouration and optical properties make electrochromic materials suitable for a wide array of applications that require visible colour-changing indicators or modulation of external light. This section critically reviews state-of-the-art electrochromic applications along with several performance parameters and their cost-efficiency. A comparative list of the performance parameters and their facile synthesis methods is given in Table 2.

6.1. Electrochromic smart windows

Electrochromic coatings can provide an efficient way of addressing building energy consumption needs by electrically modulating the transmission of incoming light through windows.[225] One of the key factors for optimal electrochromic windows is their colouration efficiency and durability.[226] To date, many electrochromic materials have been used in their pristine and tuned or modified forms to demonstrate smart coatings for windows in practical real world applications, finding their space in the commercial world like Sageglass from Saint-Gobain,[227] View,[228] Kinestral[229] and IQglass[230] to name a few. These commercial companies dominate the market with improved technologies for smart buildings like the glazing solution,[227] AI-driven enhancement[228] and grey-tint[229] for architectural integration. The commercial electrochromic glass market has seen a significant growth globally, with a projected compound annual growth rate (CAGR) of 9%, reaching $4.13 billion by 2033, according to straits research reports.[231] Several electrochromic windows have been reported with high colouration efficiency.[232–235] The PEDOT:PSS and PANI:PSS based coatings reported a CE of 1872.8 cm^2 C^{-1} at 600 nm (ref. 234) with an overall low power consumption for the colouration and bleaching processes.[234]

The introduction of PANI:PSS into the ECD results in improved chromaticity, as it results in higher optical density with fewer charge insertions.[234] Moreover, the electrochromic film, when realised on a large scale of 500 mm^2, as shown in Fig. 5a for a proof of concept device using roll-to-roll synthesis, demonstrated switching stability for 3000 cycles.[234] However, slow colouration and bleaching times of 90 s and 110 s, respectively, were reported for the device. The use of nanostructuring for electrochromic windows by Phan *et al.* resulted in optimised fast colouration and bleaching times of 0.85 s and 1 s at 1000 nm in an EC window device due to the high aspect ratio of 1D WO_3 and NiO nanorods.[238] The switching time observed in the device was higher than in thin film-based devices with similar configurations. A shortened time for colouration and bleaching indicates improved electrochromic efficiency.[238] Moreover, the device exhibits dual-band electrochromism with high CEs of 174 cm^2 C^{-1} and 386 cm^2 C^{-1} at 680 nm and 1000 nm, respectively, due to the combined polaronic and localised surface plasmon resonance effect.[238] A viologen immobilised 2D polymer-based EC window by Wang *et al.* reported a CE of 989 cm^2 C^{-1} at 550 nm (ref. 235) with respective colouration and bleaching times of 2.8 s and 1.2 s.[235] The high electrochromic efficiency and fast switching arise from the highly crystalline nature of the film due to viologen immobilisation, an abundance of viologen moieties in the 2D polymeric system and the presence of nanopores, allowing for efficient ion intercalation.[235] Dual-band multicolour tunability is also demonstrated in other EC smart windows, with a PANI device reported by Wang *et al.* showing stability for 10 000 cycles due to the reaction kinetics of the EC film in Zn $(ClO_4)_2$/PC electrolyte and CEs of 367.1 cm^2 C^{-1} and 299.6 cm^2 C^{-1} at 633 nm and 1600 nm, respectively.[225] Despite the exceptional cycling stability and high CE, the device had slower switching times.[238] In addition to PANI, other polyarylamines,

Table 2 Applications of electrochromic devices, their performance and facile synthesis techniques

Application	Colouration efficiency (cm^2 C^{-1})	Switching time τ_b = bleach time, τ_c = colour time	Economical and large-scale production	Stability
Smart windows	1872.8 at 600 nm (ref. 234)	τ_c = 1.4 s, τ_b = 1.1 s at 633 nm (ref. 288)	Inkjet printing[289] Roll to roll printing[234]	2500 cycles at 633 nm (ref. 288)
Electrochromic supercapacitor	707 at 500 nm (ref. 205)	τ_c = 0.8 s, τ_b = 0.4 s at 700 nm (ref. 257)	Solvothermal method[290]	20 000 cycles at 635 nm (ref. 260)
Electrochromic batteries	135.5 at 750 nm (ref. 291)	τ_c = 2.5 s, τ_b = 2.6 s 750 nm (ref. 291)	Facile electrochemical copolymerization process[292]	2500 cycles (ref. 291)
Electrochromic displays	560.6 at 600 nm (ref. 44)	τ_c = 447 ms, τ_b = 650 ms at 600 nm (ref. 44) Response time = 100 ms (ref. 293)	Chemical oxidative polymerization[44] Electropolymerization[270]	1500 cycles at 550 nm (ref. 162)
Electrochromic sensors	Not mentioned	Response time = 60 minutes (ref. 278)	Molecular imprinting[294] Screen printing[271]	162 cycles (ref. 295)
Electrochromic mirror	125 at 550 nm (ref. 244)	τ_c = 1.7 s, τ_b = 5.4 s at 550 nm (ref. 243)	Not mentioned	15 cycles at 515 nm (ref. 243)
Electrochromic biomimetic devices	119.2 at 633 nm (ref. 283)	τ_c = 4.1 s, τ_b = 2.9 s at 633 nm (ref. 283)	Not mentioned	100 cycles (ref. 283)

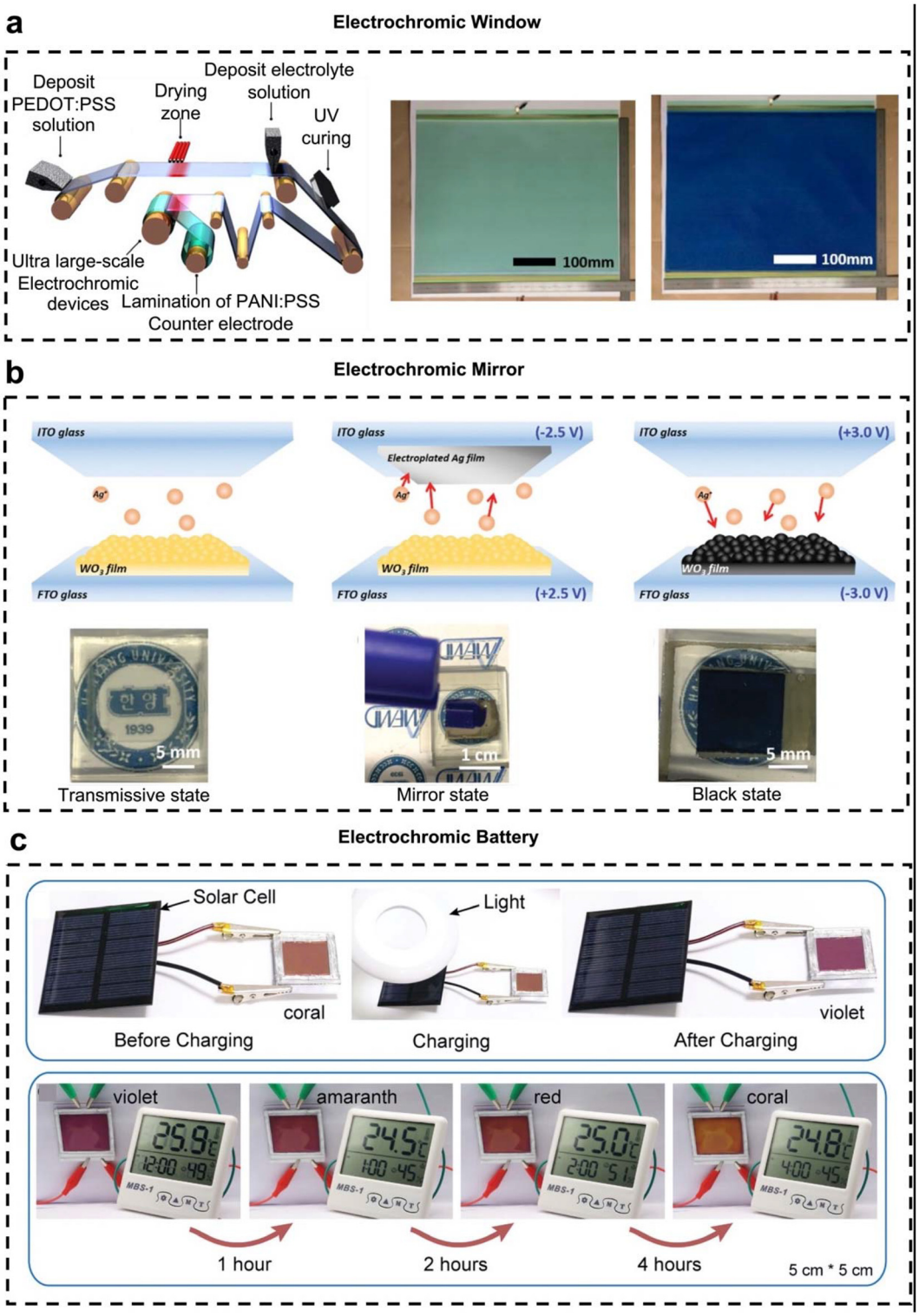

Fig. 5 Electrochromic applications. (a) 3D schematic of the roll-to-roll synthesis of a large-scale ECD for EC window applications and colour changes of the ECD in voltage off and on states, respectively. Reprinted with permission from ref. 234. Copyright 2021 American Chemical Society. (b) A 3D schematic representation of a reversible electrodeposited electrochromic mirror based on WO_3 and Ag nanoparticles in its transparent, mirror and black states, respectively. Reprinted with permission from ref. 236. Copyright 2021 Wiley. (c) Photographs of a Mn_2O_3 electrochromic battery undergoing colour changes with solar-cell charging and powering a timer while indicating different states with varying colouration while discharging. Reprinted with permission from ref. 237. Copyright 2021 Wiley.

such as poly(diphenylamine) (PDPA), have been explored for electrochromic applications.[239,240] PDPA is a p-type conjugated polymer structurally similar to PANI, offering a more favourable redox potential window and exhibiting promising visible to NIR modulation capabilities. This makes it a strong candidate for a high solar modulating ability in EC devices. Self-powered EC devices are widely investigated to reduce energy requirements for the electrical energy-driven chromic effect.[241] In a study by Wang *et al.*, EC nanowire films of $Ag/W_{18}O_{49}$ were immersed in a galvanic cell with aluminium as a counter electrode.[242] In the presence of $AlCl_3$ electrolyte, which showed colouration upon bias application due to the formation of Al^{3+} that resulted in ion intercalation.[242] The device demonstrated bleaching when no potential was applied due to the extraction of Al ions, suggesting that the device was self-powered.[242]

6.2. Electrochromic mirrors

Electrochromic materials have been widely employed in constructing electrochromic mirrors for automotive purposes, mirror-based smart windows and glasses.[243–245] The looming Orion augmented reality (AR) glasses, which will be made accessible to the public by leading tech companies like Meta (with Ray-Ban),[246] Samsung, Apple and Google,[247,248] show the versatility and datedness of research efforts that have gone into this field to date.[249] For safety concerns in the automotive industry, electrochromic mirror images have to be clearly visible during both bleaching and colouration processes.[244] The magnesium fluoride (MgF_2) antireflection layer coating on an electrochromic mirror by Kim *et al.* improved the transmission of the fluorine-doped tin oxide (FTO) substrate, improving the overall colouration efficiency of the device and resulting in a clean visible image during both colouration and bleaching states.[244] Electrochromic mirror devices for privacy-based smart windows have been developed in recent years, where the mirror and dark states are applicable for privacy reasons.[236,250] Son *et al.* demonstrated an electrochromic mirror device capable of switching between a transparent, highly reflective state and a zero-reflective dark state.[236] The device comprised of a WO_3 nanoparticle thin film layer on FTO and a Ag layer on ITO, as shown in Fig. 5b.[236] The rough surface morphology of the WO_3 layer results in the localized surface plasmon resonance (LSPR) effect upon the application of a negative bias to the WO_3 electrode, which results in the Ag nanoparticles electrodepositing onto the rough film surface, causing incident light to scatter and result in the dark state.[236] Upon the application of a positive voltage, the Ag^+ ions migrate back to the ITO electrode, resulting in the mirror state.[236] The device required approximately 16 s and 35 s to achieve its mirror and dark states and 200 s to reach its transparent state and demonstrated stability for 100 cycles.[236] In another demonstration of an electrochromic mirror capable of switching between different optical states, a CuSn device developed by Lee-Sie Eh *et al.* demonstrated a cycling stability of 1000 cycles in its reflective state and 2400 cycles in its transmissive state.[250] The device operated on the principle of electrodeposition and dissolution of the Cu and Sn alloy based on the redox reaction of the compounds in the electrolyte.[250] Upon the application of a negative potential of 1.2 V, the Cu and Sn alloy electrodeposited on the electrode, resulting in a reflective state,[250] whereas the greyish state could be attributed to the presence of greyish SnO and blue CuCl at −0.9 V.[250] The device showed superior stability, as the alloying of Sn prevented the dissolution of Cu and device degradation.[250] Some of the EC mirrors have found their place in the commercial space like the Gentex electrochromic (EC) mirrors.[251] They are self-adaptable (can also be manually controlled) dimmable mirrors for cars and aircrafts.[251]

6.3. Electrochromic energy storage device

Electrochromic materials, when integrated into an energy storage device, offer the ability to visually monitor the level of stored charge in the system.[252] Furthermore, the entire electrochromic process is an electrically driven mechanism that requires energy consumption.[253] Since it involves a redox reaction, it can enable energy harvesting,[254,255] where electrical energy applied for bleaching/colouration can be stored and utilised to drive the opposite process, making the system more energy efficient.[253] For next-generation energy storage functionalities, supercapacitors are a favourable choice due to their fast discharging and charging capabilities and extended lifetimes.[256] To be compatible with the fast charging and discharging capabilities, electrochromic supercapacitors require fast response times to visually depict the change in colour with charging state. Nanostructuring, such as introducing mesoporosity into a film, can provide a pathway for a faster ion intercalation mechanism.[257] In a study by Kim and co-workers, a mesoporous WO_3-based supercapacitor reported sub-second colouration and bleaching times.[257] Composite organic conducting polymers and metal oxide-based electrochromic supercapacitors report high colouration efficiency, which arises from their complementary electrical and optical properties that are superior to those of the pristine materials.[17,205] The high colouration efficiency of 707 $cm^2\ C^{-1}$ at 500 nm in the poly(3,4-ethylenedioxypyrrole) (PEDOP)–gold (Au)@WO_3 electrochromic supercapacitor arises from the simultaneous colouration and bleaching of WO_3 and PEDOP, thus providing a higher degree of optical modulation than their individual counterparts.[205] Several polymer-based electrochromic supercapacitors have shown fast response times, resulting from nanostructuring and the utilisation of donor–acceptor separation.[256,258,259] A stable electrochromic performance for 20 000 cycles and stable capacity retention for 50 000 cycles were shown in an electrochromic supercapacitor by Yun and co-workers.[260] Here, WO_3 nanotubes were coated with PEDOT:PSS to avoid crack formation in the WO_3 nanotubes, improving their reliability. It can be observed that, despite WO_3's excellent electrochromic and capacitive properties, its ability to only change to a single colour requires it to be composited with other chromophores for multiple colouration states.[261] Electrochromic materials employed to design batteries not only enable a visual representation of the energy levels in the battery for smart electronic devices[237] but also recycle the con-

sumed energy for energy-efficient devices.[262] Multivalent cation-based electrolytes are often preferred over monovalent ions for electrochromic batteries due to faster switching kinetics and higher charge density during redox reactions.[262] Zinc ion-based batteries have been widely reported due to their cost-efficiency and compatibility with other electrolytes.[131,262,263] A Zn ion battery with a Mn_2O_3 electrochromic layer reported by Tang *et al.* demonstrated different colours with different levels of stored charge.[237] The developed battery was also used to demonstrate its energy recycling capability with the use of a solar cell and a timer, as shown in Fig. 5c.[237] The device is initially coral (in its discharged state) and when charged using a solar cell turns violet (in its charged state).[237] During the discharging process, the device powers a timer for 4 h, during which time different coloured states visually indicate the charging level.

6.4. Electrochromic displays

EC displays utilise the electrochromic redox reaction process to switch from a highly transmissive state to a highly absorptive state and *vice versa*.[264] In contrast to displays such as LEDs and LCDs that operate in emissive mode, EC displays maintain the contents of the display without the need for an external power source due to the presence of the memory effect.[265,266] The colouration of EC displays based on inherently singular EC materials does not usually provide the multi-colouration effect.[266] Although EC displays based on metal–organic frameworks and organic materials have displayed multi-colouration properties, they come with shortcomings such as poor chemical and thermal stability.[266,267] In recent years, inorganic material-based multicolour displays have been reported.[266,267] In a report by Zhang *et al.*, a single SVO electrode/Zn-based structure demonstrated the capability for self-powered 3-state colouration with the energy retrieved from the bleaching process.[267] Hence, an EC display was further developed by overlaying two SVO electrodes between Zn for a self-powered 6-colour palette display.[267] However, the time required for switching between coloured and bleached states was too long.[267] In a subsequent study by Zhang *et al.*, one of the SVO electrodes was replaced with an asymmetric Fabry-Perot cavity WO_3 electrode for a multicolour reflective display and WO_3 film for a transparent display.[266] As seen from Fig. 6a, both devices showed 16 colour palettes due to the overlay of colour between the two independently colourable and bleachable electrodes.[266] The rapid switching of colour states is a very important factor for displays, hence obtaining ECDs with fast response times is viable.[268] A multicolour EC display based on PANI and a complementary viologen (1-methyl-4,4′-bipyridyl iodide) electrode was investigated by Liu *et al.*[269] The device demonstrated colouration and bleaching times of 1 s and 1.9 s, respectively, and a CE of 140.63 $cm^2\ C^{-1}$ at 550 nm, as shown in Fig. 6b.[269] The complementary electrode of viologen also acts as an ion storage layer that balances out excess charges thus optimising the device performance.[269] However, with time, the EC displays show a degradation in performance that is possibly due to the partial dissolution of PANI or degradation of the polymeric chain.[269] Flexible EC displays are also an important application of EC technology due to their ability to be integrated with wearable technology and IR applications.[270] A fluorophenyl-modified polythiophene electrochromic layer with a CE of 752 $cm^2\ C^{-1}$, when integrated into a flexible EC display, demonstrated performance retention for 5000 bending cycles.[270] However, the device demonstrated only a single state of colouration.[270]

6.5. Electrochromic sensors

Due to their energy efficiency and reversible colouration mechanism, electrochromic materials are becoming an integral part of developing analytical devices like self-powered sensors, as they provide an easily accessible sensor readout system.[271,272] One such application is their use in point-of-care devices for easy detection due to the easy readout features based on colourimetric changes.[273] Various studies have reported such point-of-care systems based on electrochromic readout sensors.[273–275] A self-powered electrochromic cancer biomarker sensor consisting of an electrochromic PEDOT-based film that was interfaced with a photovoltaic device was reported by Tavares *et al.*[276] The concentration of biomarker impacted the energy generation of the photovoltaic cell, which in turn controlled the colouration of the electrochromic material,[276] with no biomarker resulting in the highest power generation and palest colouration of the electrochromic sensor and higher concentrations resulting in darker colouration.[276] Other than point-of-care devices, electrochromic sensors have also been developed for detecting pathogens.[277] For instance, a PANI-based immune sensor was used for the selective, rapid detection and visual analysis of *E. coli* levels in water.[278] With an average switching time of PANI between its different redox states being 0.4 s,[278] the accumulation of different concentrations of *E. coli* bacteria resulted in different levels of colouration based on the change in the sensor circuit resistance, as shown in Fig. 6c.[237,278] Similarly, using the redox property of PB, a self-powered sensor for detecting toxins in wastewater was demonstrated by Yu *et al.*[279] PB acted as a cathode, whereas the anode was a microbe, whose activity was dependent on respiratory changes in the microorganism in the presence of toxins.[279] With toxins present in the water, the respiration of the microorganism was inhibited, which slowed down electron transfer in the cell, resulting in a lighter blue colour and preventing the conversion of PB into Prussian white with a cycling stability of 162 cycles.[279] The device demonstrates varying absorbance changes to different toxins, indicating its capability to detect heavy metals in wastewater.[279]

6.6. Electrochromic biomimetic devices

Electrochromic materials have been widely employed in various biomimetic applications such as self-healing chameleon/camouflage skin,[280–282] actuators,[283] artificial muscles,[284] camouflage materials[285,286] and tissues.[287] Electrochromic actuators can often provide a way to fabricate colour-altering

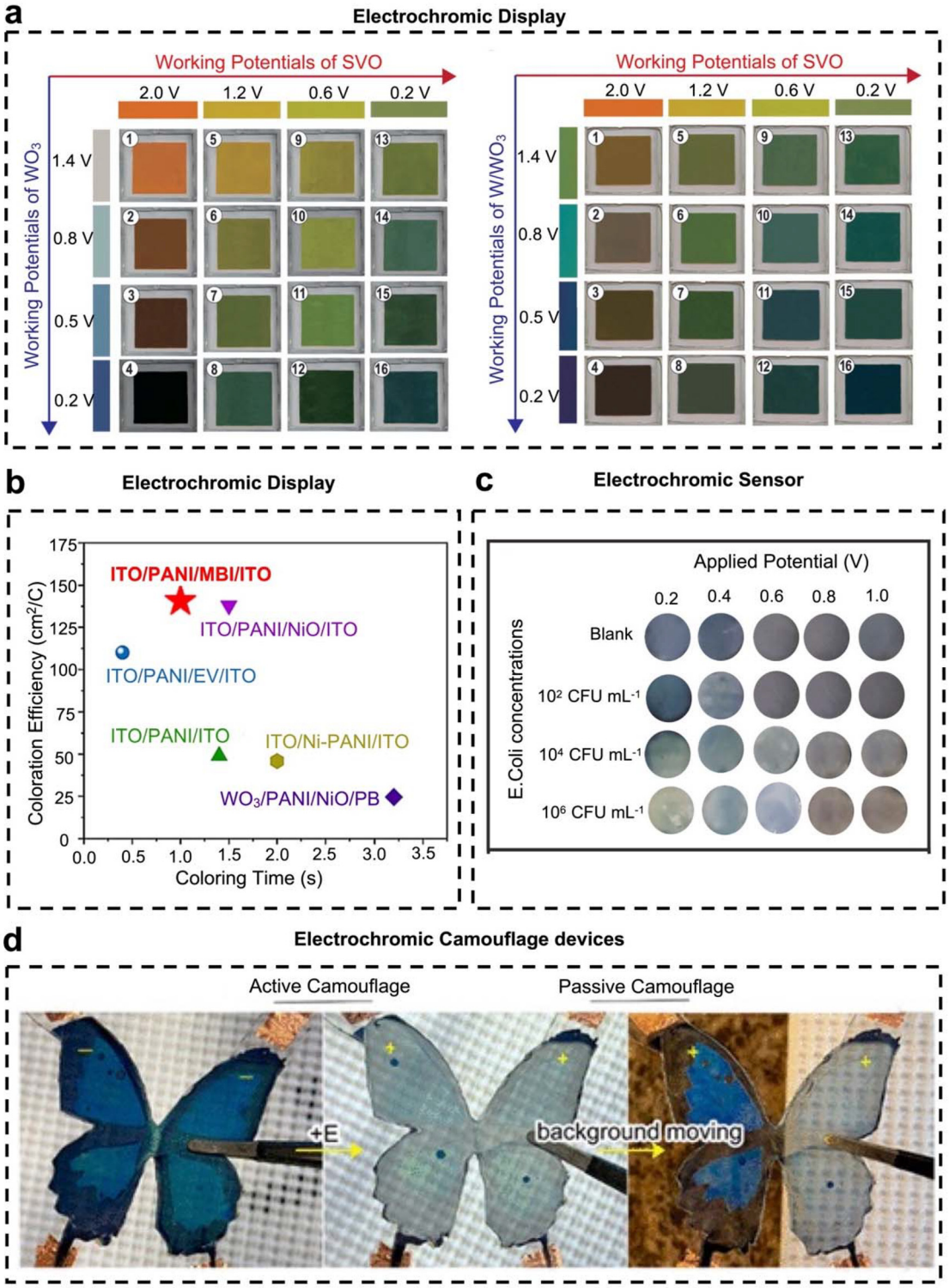

Fig. 6 Electrochromic visual applications. (a) Optical photographs of both transmissive and reflective displays based on SVO–Zn–WO_3 and SVO–Zn–W/WO_3 using the colour overlay effect, resulting in 16 colour palettes on a single device with varying potentials. Reprinted with permission from ref. 266. Copyright 2022 Wiley. (b) A complementary electrochromic display based on PANI and viologen indicates higher colour efficiency and a faster switching time than other organic electrochromic material-based displays due to the presence of a complementary viologen layer. Reprinted with permission from ref. 269. Copyright 2024 Elsevier. (c) A visual PANI-based electrochromic sensor for detecting *E. coli* concentrations where the device indicates a change in colouration with varying *E. coli* concentration and the potential applied. Reprinted with permission from ref. 278. Copyright 2019 American Chemical Society. (d) A glass/ITO/EC polymer/silica-nanoparticle-LiTFSI-PC-PEGDA/Nb_2O_5/ITO/glass camouflage device demonstrating active camouflage (electrochromic colour change) controlled by bias voltage and in its bleached state showing passive camouflage due to the interaction of plasmonic nanocrystals embedded in the system with the reflective background. Reprinted with permission from ref. 280. Copyright 2021 American Chemical Society.

chameleon skin.[140] A lattice contraction–de-contraction phenomenon occurring due to ionic intercalation and de-intercalation, resulting in a pseudocapacitive deformation of tungsten oxide ($W_{18}O_{49}$) nanowires, was reported by Li *et al.* This results in a simultaneously occurring contraction–relaxation process along with electrochromic colour changes, thereby acting as an electrochromic actuator.[283] The actuator shows a high CE and a rapid colouration time of 4.1 s and bleaching time of 2.9 s, which can be attributed to the interconnected micro–nanochannels that reduce the ion traversal path.[283] Electrochromic actuation arising from the dimensional changes occurring in PANI during electrochromic optical modulation can lead to the development of optical signal-generating artificial muscles.[287] In a study by Chen *et al.*, electrochromic camouflage skin was devised using an architecture of glass/ITO/EC polymer/silica-nanoparticle-LiTFSI-PC-PEGDA/Nb_2O_5/ITO/glass.[280] The EC polymer (PProDOTBT, ECP-black) under a bias of −1.3 V remains in its dark state, where light reflection arises from the nanoparticles, making the device look green.[280] However, with increasing field, the polymer becomes transmissive and this overpowers the reflection from the nanocrystals, making the device transparent.[280] This reflective surface camouflage property is further evident from Fig. 6d.[280] As observed, the device has both active camouflage properties, where it can be coloured and transparent under an external electric field,[280] and passive camouflage properties, where the transmissive device, under a reflective surface like marbles in comparison with paper, demonstrates colouration controlled by reflection from the silica nanoparticles.[280] Table 2 presents the different types of electrochromic applications, the performance efficiencies of various devices and the synthesis mechanisms.

7. Conclusion and outlook

There have been substantial advancements in the field of electrochromism in the past decade wherein electrochromic materials have been widely used in various applications ranging from energy-efficient smart windows to displays. This review has provided insights into the underlying governing principle of electrochromic behaviour in different materials, their degradation reversal strategies and their performance optimization using strategies such as nanostructuring, doping and compositing. Several studies have investigated the use of structural modulation to optimise electrochromic material characteristics. For instance, the use of nanostructuring has been shown to have a beneficial impact on electrochromic properties due to (i) the improved specific surface area for improved material–electrolyte contact, (ii) a larger number of intercalation sites due to permeable channels in nanostructured materials and (iii) shortened ion traversal lengths. The use of nanostructured composite materials has been shown to lead to highly efficient electrochromic systems with synergistic material properties resulting from individual electrochromic materials.

There is also often a decrease in the performance parameters of electrochromic devices with increasing size of the device. Hence, there need to be more efforts made to utilise cost-efficient nanostructuring methods for large-scale production of nanostructured composite electrochromic material systems. Also, improved design aspects are essential factors for addressing these challenges, although there is often low colouration with multivalent ions compared to traditional lithium-based ion intercalation. Given the improved cycling stability occurring with multivalent ions, a trade-off can be made for commercialising electrochromic devices. Furthermore, these modulation strategies have been expanded to electrochromic application scenarios that have resulted in improved device performance.

While electrochromic materials and devices show promising potential for various applications, their widespread commercialization faces several challenges related to cost, performance, and cycling stability. One of the primary hurdles is the trade-off between the cost of production and device performance. Devices fabricated using economical technologies often suffer from slower response speeds and poorer durability and stability, which can limit their practical application. To enable large-scale commercialization, it is crucial to reduce production costs while maintaining optimum performance and stability.

The stability of electrochromic devices is another critical factor that needs to be addressed. Many electrochromic materials and devices exhibit limited cycle life, which is not viable for day-to-day applications. Strategies to counteract the fast degradation of these devices are essential for successful commercialization. This may involve developing new materials with improved stability, optimizing device architectures, or incorporating protective coatings and encapsulation techniques. As such, there is significant room for research into pathways that enhance the scalability and durability of 2D nanostructures. With the emergence of new scalable fabrication and encapsulation strategies for such nanostructures, there is now an opportunity to explore these material systems further to assess their practical value either alone or in combination with existing systems.

Future prospects for electrochromic technologies lie in addressing these challenges through innovative material design, device engineering, and manufacturing processes. The development of cost-effective, high-performance electrochromic materials with tailored properties is a key area of focus. Advancements in nanostructuring, compositing, and doping strategies can potentially enhance the electrochromic performance while maintaining affordability.

Electrochromic materials hold significant potential for advancing NIR/IR technologies due to their ability to dynamically modulate light in optical communication systems (*e.g.*, ultrafast variable optical attenuators) and enable novel applications in the aerospace, healthcare, and defense (*e.g.*, multispectral military camouflage) fields. These materails adapt to visible, NIR, and thermal IR bands through tunable emissivity and reflectivity, offering compatibility with evolving multispec-

tral detection systems. The advancements in EC conducting polymers and transition metal oxides will improve their performance and durability, while emerging technologies like plasmonic metasurfaces and MXene–conducting polymer composites will expand the material landscape. As the technology matures, electrochromic materials are expected to converge with other emerging technologies, such as flexible electronics, internet of things (IoT), artificial intelligence and energy-efficient buildings, presenting exciting opportunities for new applications. Smart windows and displays with dynamic control over light and heat transmission can significantly contribute to energy savings and user comfort.

Collaborative efforts between academia, industry, and government agencies are crucial to accelerate the commercialization of electrochromic technologies. Initiatives focused on scaling up production, establishing industry standards, and addressing regulatory requirements will play a vital role in bringing these technologies to the market. Additionally, public awareness and acceptance of electrochromic products will be essential for their widespread adoption.

Data availability

This review is based on critical analysis of the existing literature. No original research findings, software, or code have been included and no new data were generated, collected, or analyzed in the preparation of this review.

Conflicts of interest

There are no conflicts to declare.

Acknowledgements

The authors acknowledge support from the Australian Research Council Discovery Project DP220100020 (S. W., E. D. G., and I. H. A.) and DP240100145 (S. W., and I. H. A.). T. A. and S. W., acknowledge support from Office of National Intelligence (NI230100026).

References

1 H. Liang, R. Li, C. Li, C. Hou, Y. Li, Q. Zhang and H. Wang, *Mater. Horiz.*, 2019, **6**, 571–579.
2 M. Pan, Y. Ke, L. Ma, S. Zhao, N. Wu and D. Xiao, *Electrochim. Acta*, 2018, **266**, 395–403.
3 F.-H. Liu, J. Bai, G. Yu, F.-H. Ma, Y.-J. Hou and H.-J. Niu, *Org. Electron.*, 2020, **77**, 105538.
4 H. Xu, L. Gong, S. Zhou, K. Cao, S. Wang, J. Zhao and Y. Li, *New J. Chem.*, 2020, **44**, 2236–2240.
5 M. R. Scherer, L. Li, P. M. Cunha, O. A. Scherman and U. Steiner, *Adv. Mater.*, 2012, **24**, 1217–1221.
6 H. Gu, C. Guo, S. Zhang, L. Bi, T. Li, T. Sun and S. Liu, *ACS Nano*, 2018, **12**, 559–567.
7 A. Hasani, Q. V. Le, T. P. Nguyen, K. S. Choi, W. Sohn, J. K. Kim, H. W. Jang and S. Y. Kim, *Sci. Rep.*, 2017, **7**, 13258.
8 A. Arash, S. A. Tawfik, M. J. S. Spencer, S. Kumar Jain, S. Arash, A. Mazumder, E. Mayes, F. Rahman, M. Singh, V. Bansal, S. Sriram, S. Walia, M. Bhaskaran and S. Balendhran, *ACS Appl. Mater. Interfaces*, 2020, **12**, 16997–17003.
9 P. Jittiarporn, L. Sikong, K. Kooptarnond, W. Taweepreda, S. Stoenescu, S. Badilescu and V.-V. Truong, *Surf. Coat. Technol.*, 2017, **327**, 66–74.
10 A. Kumar, C. S. Prajapati and P. Sahay, *Mater. Sci. Semicond. Process.*, 2019, **104**, 104668.
11 Y. Chen, Z. Bi, X. Li, X. Xu, S. Zhang and X. Hu, *Electrochim. Acta*, 2017, **224**, 534–540.
12 H.-T. Zhang, P. Subramanian, O. Fussa-Rydel, J. C. Bebel and J. T. Hupp, *Sol. Energy Mater. Sol. Cells*, 1992, **25**, 315–325.
13 M. D. Ward, *J. Solid State Electrochem.*, 2005, **9**, 778–787.
14 A. Kraft, *Sol. Energy Mater. Sol. Cells*, 2024, **278**, 113195.
15 K. Tang, Y. Zhang, Y. Shi, J. Cui, X. Shu, Y. Wang, J. Liu, J. Wang, H. H. Tan and Y. Wu, *J. Mater. Chem. C*, 2018, **6**, 12206–12216.
16 S. Zhang, G. Sun, Y. He, R. Fu, Y. Gu and S. Chen, *ACS Appl. Mater. Interfaces*, 2017, **9**, 16426–16434.
17 Q. Guo, X. Zhao, Z. Li, D. Wang and G. Nie, *Chem. Eng. J.*, 2020, **384**, 123370.
18 A. Azam, J. Kim, J. Park, T. G. Novak, A. P. Tiwari, S. H. Song, B. Kim and S. Jeon, *Nano Lett.*, 2018, **18**, 5646–5651.
19 M. Ojha, R. Mysoon, A. K. Ray, G. S. Rongali and M. Deepa, *Sol. Energy Mater. Sol. Cells*, 2024, **269**, 112797.
20 M. Hassan, A. Ghaffar, G. Lou, Z. Miao, Z. Peng and K. Celebi, *Adv. Funct. Mater.*, 2024, **34**, 2310535.
21 M. Hassan, P. Li, J. Lin, Z. Li, M. S. Javed, Z. Peng and K. Celebi, *Small*, 2024, **20**, 2400278.
22 J. Chen, B. Xu, Y. Zhang, W. Zhang, H. Wang, A. Y. Elezzabi, L. Liu, W. W. Yu and H. Li, *Appl. Phys. Rev.*, 2024, **11**, 011316.
23 F. Zhao, B. Wang, W. Zhang, S. Cao, L. Liu, A. Y. Elezzabi, H. Li and W. W. Yu, *Mater. Today*, 2023, **66**, 431–447.
24 Y. Liu, L. Huang, S. Cao, J. Chen, B. Zou and H. Li, *Nanophotonics*, 2024, **13**, 155–172.
25 Y. Yao, Q. Zhao, W. Wei, Z. Chen, Y. Zhu, P. Zhang, Z. Zhang and Y. Gao, *Nano Energy*, 2020, **68**, 104350.
26 S. Zhao, W. Huang, Z. Guan, B. Jin and D. Xiao, *Electrochim. Acta*, 2019, **298**, 533–540.
27 K. Łępicka, P. Pieta, A. Shkurenko, P. Borowicz, M. Majewska, M. Rosenkranz, S. Avdoshenko, A. A. Popov and W. Kutner, *J. Phys. Chem. C*, 2017, **121**, 16710–16720.
28 L.-M. Huang, T.-C. Wen and A. Gopalan, *Synth. Met.*, 2002, **130**, 155–163.
29 C.-L. Lin, C.-C. Lee and K.-C. Ho, *J. Electroanal. Chem.*, 2002, **524–525**, 81–89.

30 S.-H. Lee, H. M. Cheong, C. E. Tracy, A. Mascarenhas, J. R. Pitts, G. Jorgensen and S. K. Deb, *Appl. Phys. Lett.*, 2000, **76**, 3908–3910.
31 V. B. Isfahani, N. Memarian, H. R. Dizaji, A. Arab and M. M. Silva, *Electrochim. Acta*, 2019, **304**, 282–291.
32 S. Y. Chun, S. Park, S. I. Lee, H. D. Nguyen, K.-K. Lee, S. Hong, C.-H. Han, M. Cho, H.-K. Choi and K. Kwak, *Nano Energy*, 2021, **82**, 105721.
33 T. Pauporté and R. Durand, *J. Appl. Electrochem.*, 2000, **30**, 35–41.
34 C. C. Chen, *J. Nanomater.*, 2013, **2013**, 1–14.
35 R. Ahmad, N. O. Laschuk, I. I. Ebralidze, O. V. Zenkina and E. B. Easton, *ChemElectroChem*, 2021, **8**, 2193–2204.
36 W. Zhang, H. Li, E. Hopmann and A. Y. Elezzabi, *Nanophotonics*, 2020, **10**, 825–850.
37 Y. Wu, Y. K. Mishra and J. Xiong, *Color. Technol.*, 2023, **140**, 208–229.
38 H.-Y. Liao, T.-C. Liao, W.-H. Chen, C.-H. Chang and L.-C. Chen, *Sol. Energy Mater. Sol. Cells*, 2016, **145**, 8–15.
39 R. J. Mortimer, D. R. Rosseinsky and P. M. Monk, *Electrochromic materials and devices*, John Wiley & Sons, 2015.
40 C. R. Dhas, R. Venkatesh, R. Sivakumar, T. Dhandayuthapani, B. Subramanian, C. Sanjeeviraja and A. M. E. Raj, *J. Alloys Compd.*, 2019, **784**, 49–59.
41 I. Perez, J. C. Martínez Faudoa, J. R. Abenuz Acuña and J. T. Elizalde Galindo, *Comput. Mater. Sci.*, 2021, **190**, 110248.
42 H. Ling, J. Lu, S. Phua, H. Liu, L. Liu, Y. Huang, D. Mandler, P. S. Lee and X. Lu, *J. Mater. Chem. A*, 2014, **2**, 2708–2717.
43 T. G. Novak, J. Kim, A. P. Tiwari, J. Kim, S. Lee, J. Lee and S. Jeon, *ACS Sustainable Chem. Eng.*, 2020, **8**, 11276–11282.
44 S. Zhang, J. Ren, S. Chen, Y. Luo, X. Bai, L. Ye, F. Yang and Y. Cao, *J. Electroanal. Chem.*, 2020, 114248.
45 Y.-M. Zhang, X. Wang, W. Zhang, W. Li, X. Fang, B. Yang, M. Li and S. X.-A. Zhang, *Light: Sci. Appl.*, 2015, **4**, e249–e249.
46 J. Jiang, L. Qin, J. Halim, P. O. Persson, L. Hou and J. Rosen, *Nano Res.*, 2022, 1–7.
47 Y. Cai, X. Chen, Y. Xu, Y. Zhang, H. Liu, H. Zhang and J. Tang, *Carbon Energy*, 2024, e501.
48 K. Ma, Q. Tang, C.-R. Zhu, J.-F. Long, C.-B. Gong and X.-K. Fu, *Electrochim. Acta*, 2018, **259**, 986–993.
49 Y. Alesanco, A. Viñuales, J. Ugalde, E. Azaceta, G. Cabañero, J. Rodriguez and R. Tena-Zaera, *Sol. Energy Mater. Sol. Cells*, 2018, **177**, 110–119.
50 I. I. Ebralidze and O. V. Zenkina, *Chem*, 2021, **7**, 1146–1148.
51 M. Qiu, F. Zhou, P. Sun, X. Chen, C. Zhao and W. Mai, *Nano Energy*, 2020, 105148.
52 C.-A. Tao, Y. Li and J. Wang, *Coord. Chem. Rev.*, 2023, **475**, 214891.
53 W. Wu, M. Wang, J. Ma, Y. Cao and Y. Deng, *Adv. Electron. Mater.*, 2018, **4**, 1800185.
54 G. J. Stec, A. Lauchner, Y. Cui, P. Nordlander and N. J. Halas, *ACS Nano*, 2017, **11**, 3254–3261.
55 T. Abidin, Q. Zhang, K.-L. Wang and D.-J. Liaw, *Polymer*, 2014, **55**, 5293–5304.
56 A. Dewan, S. Sur, R. Narayanan and M. O. Thotiyl, *ChemElectroChem*, 2022, **9**, e202200001.
57 J. Dong, S. Cui, F. Wang, W. Wei, Z. Yin, Y. Zhang and Q. Zhu, *Ionics*, 2024, **30**, 1615–1625.
58 J. Liu, X. Y. Daphne Ma, Z. Wang, L. Xu, T. Xu, C. He, F. Wang and X. Lu, *ACS Appl. Mater. Interfaces*, 2020, **12**, 7442–7450.
59 J.-P. Liu, C.-R. Zhang, L.-K. Li and S.-Q. Zang, *Cryst. Growth Des.*, 2024, **24**, 3299–3308.
60 N. Zhang, Y. Jin, Q. Zhang, J. Liu, Y. Zhang and H. Wang, *Ionics*, 2021, **27**, 3655–3662.
61 S. W. Tong, J. Chai, M.-F. Ng, W. Fu, W. P. Goh and C. Jiang, *ACS Appl. Opt. Mater.*, 2024, **2**, 539–548.
62 A. Mazel, M. Fornasarig, J. Owona, L. Truflandier, F. Castet and A. Rougier, *Dalton Trans.*, 2024, **53**, 1657–1662.
63 S. Cong, Y. Tian, Q. Li, Z. Zhao and F. Geng, *Adv. Mater.*, 2014, **26**, 4260–4267.
64 D. S. Dalavi, R. S. Devan, R. A. Patil, R. S. Patil, Y.-R. Ma, S. B. Sadale, I. Kim, J.-H. Kim and P. S. Patil, *J. Mater. Chem. C*, 2013, **1**, 3722–3728.
65 S. Santhosh, M. Mathankumar, S. Selva Chandrasekaran, A. K. Nanda Kumar, P. Murugan and B. Subramanian, *Langmuir*, 2017, **33**, 19–33.
66 L. Zheng, Y. Xu, D. Jin and Y. Xie, *Chem. Mater.*, 2009, **21**, 5681–5690.
67 T. Dhandayuthapani, R. Sivakumar, R. Ilangovan, C. Gopalakrishnan, C. Sanjeeviraja and A. Sivanantharaja, *Electrochim. Acta*, 2017, **255**, 358–368.
68 R. A. Patil, R. S. Devan, Y. Liou and Y.-R. Ma, *Sol. Energy Mater. Sol. Cells*, 2016, **147**, 240–245.
69 D. Nunes, T. Freire, A. Barranger, J. Vieira, M. Matias, S. Pereira, A. Pimentel, N. J. Cordeiro, E. Fortunato and R. Martins, *Appl. Sci.*, 2020, **10**, 1200.
70 Z. W. Fu and Q. Z. Qin, *Electrochem. Solid-State Lett.*, 1998, **2**, 600.
71 S.-C. Wang, K.-Y. Liu and J.-L. Huang, *Thin Solid Films*, 2011, **520**, 1454–1459.
72 X. Xia, J. Tu, J. Zhang, J. Xiang, X. Wang and X. Zhao, *Sol. Energy Mater. Sol. Cells*, 2010, **94**, 386–389.
73 C. R. Dhas, R. Venkatesh, R. Sivakumar, A. M. E. Raj and C. Sanjeeviraja, *Opt. Mater.*, 2017, **72**, 717–729.
74 X. Xia, J. Tu, J. Zhang, X. Huang, X. Wang and X. Zhao, *Electrochim. Acta*, 2010, **55**, 989–994.
75 D. Zhou, B. Che and X. Lu, *J. Mater. Chem. C*, 2017, **5**, 1758–1766.
76 X. Xia, J. Tu, J. Zhang, X. Wang, W. Zhang and H. Huang, *Sol. Energy Mater. Sol. Cells*, 2008, **92**, 628–633.
77 R. A. Patil, R. S. Devan, J.-H. Lin, Y.-R. Ma, P. S. Patil and Y. Liou, *Sol. Energy Mater. Sol. Cells*, 2013, **112**, 91–96.
78 Y. Yuan, X. Xia, J. Wu, Y. Chen, J. Yang and S. Guo, *Electrochim. Acta*, 2011, **56**, 1208–1212.
79 N. Özer and F. Tepehan, *Sol. Energy Mater. Sol. Cells*, 1999, **56**, 141–152.

80 T. Maruyama and T. Kanagawa, *J. Electrochem. Soc.*, 1996, **143**, 1675.
81 H. Wang, M. Yan and Z. Jiang, *Thin Solid Films*, 2001, **401**, 211–215.
82 C. Y. Jeong, Y. Abe, M. Kawamura, K. H. Kim and T. Kiba, *Sol. Energy Mater. Sol. Cells*, 2019, **200**, 109976.
83 C. Y. Jeong, Y. Abe, M. Kawamura, K. H. Kim, T. Kiba, H. Watanabe, K. Tajima and T. Kawamoto, *Thin Solid Films*, 2020, **709**, 138226.
84 Y. Lu, L. Liu, D. Mandler and P. S. Lee, *J. Mater. Chem. C*, 2013, **1**, 7380–7386.
85 J. Qian, D. Ma, Z. Xu, D. Li and J. Wang, *Sol. Energy Mater. Sol. Cells*, 2018, **177**, 9–14.
86 V. B. Isfahani, N. Memarian, H. R. Dizaji, A. Arab and M. Silva, *Electrochim. Acta*, 2019, **304**, 282–291.
87 Z. Li, Y. Tang, K. Zhou, H. Wang and H. Yan, *Materials*, 2019, **12**, 28.
88 E. Kholoud, H. Watanabe, A. Takahashi, M. M. Emara, B. A. Abd-El-Nabey, M. Kurihara, K. Tajima and T. Kawamoto, *J. Mater. Chem. C*, 2017, **5**, 8921–8926.
89 Y.-C. Wang, H.-C. Lu, L.-Y. Hsiao, Y.-A. Lu and K.-C. Ho, *Sol. Energy Mater. Sol. Cells*, 2019, **200**, 109929.
90 N. Bhosale and A. Kadam, *Int. J. Innov. Res. Sci. Technol.*, 2016, **3**, 106–110.
91 L. Zhao, L. Zhao, Y. Xu, T. Qiu, L. Zhi and G. Shi, *Electrochim. Acta*, 2009, **55**, 491–497.
92 D. Yiğit, Y. A. Udum, M. Güllü and L. Toppare, *J. Electroanal. Chem.*, 2014, **712**, 215–222.
93 S. V. Vasilyeva, E. Unur, R. M. Walczak, E. P. Donoghue, A. G. Rinzler and J. R. Reynolds, *ACS Appl. Mater. Interfaces*, 2009, **1**, 2288–2297.
94 E. Unur, J.-H. Jung, R. J. Mortimer and J. R. Reynolds, *Chem. Mater.*, 2008, **20**, 2328–2334.
95 P. Chandrasekhar, B. J. Zay, C. Cai, Y. Chai and D. Lawrence, *J. Appl. Polym. Sci.*, 2014, **131**, 41043.
96 S.-H. Hsiao, G.-S. Liou and H.-M. Wang, *J. Polym. Sci., Part A: Polym. Chem.*, 2009, **47**, 2330–2343.
97 Z. Wang, Y. He, M. Gu, Y. Du, S. X. Mao and C. Wang, *ACS Appl. Mater. Interfaces*, 2016, **8**, 24567–24572.
98 J. Wan, S. D. Lacey, J. Dai, W. Bao, M. S. Fuhrer and L. Hu, *Chem. Soc. Rev.*, 2016, **45**, 6742–6765.
99 D. Dong, H. Djaoued, G. Vienneau, J. Robichaud, D. Brown, R. Brüning and Y. Djaoued, *Electrochim. Acta*, 2020, **335**, 135648.
100 X. Tong, J. Wang, P. Zhang, P. Lei, Y. Gao, R. Ren, S. Zhang, R. Zhu and G. Cai, *Chem. Eng. J.*, 2023, **470**, 144130.
101 J. Li, X. Wang, W. Sun, K. Maleski, C. E. Shuck, K. Li, P. Urbankowski, K. Hantanasirisakul, X. Wang, P. Kent, H. Wang and Y. Gogotsi, *ChemElectroChem*, 2021, **8**, 151–156.
102 Y. He, T. Li, X. Zhong, M. Zhou, G. Dong and X. Diao, *Electrochim. Acta*, 2019, **316**, 143–151.
103 Q.-H. Wu, A. Thißen and W. Jaegermann, *Surf. Sci.*, 2005, **578**, 203–212.
104 G. Yuan, C. Hua, L. Huang, C. Defranoux, P. Basa, Y. Liu, C. Song and G. Han, *Appl. Surf. Sci.*, 2017, **421**, 630–635.
105 Y. Wang, X. Jia, E. B. Berda, J. Zhao, X. Liu and D. Chao, *Eur. Polym. J.*, 2020, **138**, 109979.
106 J. Wu, Y. Zhu, L. You, P.-T. Dong, J. Mei and J.-X. Cheng, *Adv. Funct. Mater.*, 2020, **30**, 2005192.
107 Y. Wang, R. Shen, S. Wang, Q. Chen, C. Gu, W. Zhang, G. Yang, Q. Chen, Y.-M. Zhang and S. X.-A. Zhang, *Chem*, 2021, **7**, 1308–1320.
108 A. L.-S. Eh, M.-F. Lin, M. Cui, G. Cai and P. S. Lee, *J. Mater. Chem. C*, 2017, **5**, 6547–6554.
109 M. Qiu, F. Zhou, P. Sun, X. Chen, C. Zhao and W. Mai, *Nano Energy*, 2020, **78**, 105148.
110 S. Mishra, H. Pandey, P. Yogi, S. K. Saxena, S. Roy, P. Sagdeo and R. Kumar, *Solid State Commun.*, 2017, **261**, 17–20.
111 Q. Zhang, L. Yuan, F. Guan, X. Li, R. Wang, J. Xu, Y. Qin and G. Chen, *Materials*, 2021, **14**, 1702.
112 K. Łępicka, P. Pieta, A. Shkurenko, P. Borowicz, M. Majewska, M. Rosenkranz, S. Avdoshenko, A. A. Popov and W. Kutner, *J. Phys. Chem. C*, 2017, **121**, 16710–16720.
113 R. Shen, H. Xi, Y. Wang, G. Ren, D. Liu, Y.-M. Zhang and S. X.-A. Zhang, *J. Mater. Chem. A*, 2022, **10**, 25078–25084.
114 M. K. Bera, Y. Ninomiya and M. Higuchi, *Commun. Chem.*, 2021, **4**, 56.
115 Y. Wang, R. Shen, S. Wang, Y.-M. Zhang and S. X.-A. Zhang, *Adv. Mater.*, 2022, **34**, 2104413.
116 T. Ye, Y. Xiang, H. Ji, C. Hu and G. Wu, *RSC Adv.*, 2016, **6**, 30769–30775.
117 X. Guo, J. Chen, A. L.-S. Eh, W. C. Poh, F. Jiang, F. Jiang, J. Chen and P. S. Lee, *ACS Appl. Mater. Interfaces*, 2022, **14**, 20237–20246.
118 B. C. De Simone, M. E. Alberto, T. Marino, N. Russo and M. Toscano, *Molecules*, 2021, **26**, 5793.
119 Y. Liang, S. Cao, Y. Liu, L. He, X. Han, R. Zeng, J. Zhao and B. Zou, *Energy Mater. Adv.*, 2022, **2022**, 9878957.
120 J. Li, X. Wang, W. Sun, K. Maleski, C. E. Shuck, K. Li, P. Urbankowski, K. Hantanasirisakul, X. Wang, P. Kent, H. Wang and Y. Gogotsi, *ChemElectroChem*, 2020, **8**, 151–156.
121 H. Li, L. Zhang, H. Lin and X. Fan, *RSC Adv.*, 2014, **4**, 45635–45640.
122 T. L. da Costa Gouveia, R. B. Campos, R. R. Ribeiro and F. S. Nunes, *J. Comput. Chem.*, 2019, **40**, 1593–1598.
123 B. Faceira, L. Teule-Gay, G. M. Rignanese and A. Rougier, *J. Phys. Chem. Lett.*, 2022, **13**, 8111–8115.
124 K. M. Prasanna, A. Shukla, K. Tamizharasu, A. Ganatra, A. Shelke, A. S. M. Metwally and S. Aftab, *Opt. Quantum Electron.*, 2023, **56**, 15.
125 H. Lai, Q. Cai, M. Li, S. Kong, Y. Wu, H. Yang, Y. Zhang and H. Ning, *ACS Appl. Mater. Interfaces*, 2024, **16**, 28798–28807.
126 E. C. Gok, M. O. Yildirim, E. Eren and A. U. Oksuz, *ACS Omega*, 2020, **5**, 23257–23267.
127 R. Tällberg, B. P. Jelle, R. Loonen, T. Gao and M. Hamdy, *Sol. Energy Mater. Sol. Cells*, 2019, **200**, 109828.
128 A. Khatibi, M. Hossein Jahangir and F. Razi Astaraei, *Sol. Energy*, 2022, **241**, 671–685.

129 J. Guo, M. Wang, X. Diao, Z. Zhang, G. Dong, H. Yu, F. Liu, H. Wang and J. Liu, *J. Phys. Chem. C*, 2018, **122**, 19037–19043.
130 S. Zhang, S. Cao, T. Zhang, A. Fisher and J. Y. Lee, *Energy Environ. Sci.*, 2018, **11**, 2884–2892.
131 H. Li, L. McRae, C. J. Firby and A. Y. Elezzabi, *Adv. Mater.*, 2019, **31**, e1807065.
132 R.-T. Wen, C. G. Granqvist and G. A. Niklasson, *Nat. Mater.*, 2015, **14**, 996–1001.
133 R.-T. Wen, G. A. Niklasson and C. G. Granqvist, *ACS Appl. Mater. Interfaces*, 2016, **8**, 5777–5782.
134 I. Sorar, E. A. Rojas-González, İ. B. Pehlivan, C. G. Granqvist and G. A. Niklasson, *J. Electrochem. Soc.*, 2019, **166**, H795.
135 M. Meenakshi, V. Gowthami, P. Perumal, R. Sivakumar and C. Sanjeeviraja, *Electrochim. Acta*, 2015, **174**, 302–314.
136 K.-C. Lee, C.-W. Chang-Jian, E.-C. Cho, J.-H. Huang, W.-T. Lin, B.-C. Ho, J.-A. Chou and Y.-S. Hsiao, *Sol. Energy Mater. Sol. Cells*, 2019, **195**, 1–11.
137 L. Zhu, C. K. N. Peh, T. Zhu, Y.-F. Lim and G. W. Ho, *J. Mater. Chem. A*, 2017, **5**, 8343–8351.
138 Y. Qi, K. Qin, Y. Zou, L. Lin, Z. Jian and W. Chen, *Appl. Surf. Sci.*, 2020, 145950.
139 X. Zhou, X. Zheng, B. Yan, T. Xu and Q. Xu, *Appl. Surf. Sci.*, 2017, **400**, 57–63.
140 J. Xue, S. Wang, H. Zhang, Y. Song, Y. Li and J. Zhao, *J. Mater. Sci.: Mater. Electron.*, 2020, 1–9.
141 H. C. Lu, S. Ghosh, N. Katyal, V. S. Lakhanpal, I. R. Gearba-Dolocan, G. Henkelman and D. J. Milliron, *ACS Nano*, 2020, **14**, 10068–10082.
142 R. Li, X. Ma, J. Li, J. Cao, H. Gao, T. Li, X. Zhang, L. Wang, Q. Zhang, G. Wang, C. Hou, Y. Li, T. Palacios, Y. Lin, H. Wang and X. Ling, *Nat. Commun.*, 2021, **12**, 1587.
143 C.-A. Li, B. Ko, K.-H. Park, J.-G. Ahn, T. Park, D.-J. Lee and S.-H. Song, *Materials*, 2024, **17**, 41.
144 H. Liu, Y. Zhang, P. Lei, J. Feng, S. Jia, J. Huang, C. Hu, C. Bian and G. Cai, *ACS Appl. Mater. Interfaces*, 2023, **15**, 23412–23420.
145 S. Mondal, Y. Ninomiya, T. Yoshida, T. Mori, M. K. Bera, K. Ariga and M. Higuchi, *ACS Appl. Mater. Interfaces*, 2020, **12**, 31896–31903.
146 Q. Hao, Z.-J. Li, C. Lu, B. Sun, Y.-W. Zhong, L.-J. Wan and D. Wang, *J. Am. Chem. Soc.*, 2019, **141**, 19831–19838.
147 M. K. Bera, T. Mori, T. Yoshida, K. Ariga and M. Higuchi, *ACS Appl. Mater. Interfaces*, 2019, **11**, 11893–11903.
148 Y. Kuai, W. Li, Y. Dong, W.-Y. Wong, S. Yan, Y. Dai and C. Zhang, *Dalton Trans.*, 2019, **48**, 15121–15126.
149 S. Roy and C. Chakraborty, *ACS Appl. Mater. Interfaces*, 2020, **12**, 35181–35192.
150 S. Roy and C. Chakraborty, *ACS Appl. Mater. Interfaces*, 2020, **12**, 35181–35192.
151 Y. Liu, R. Sakamoto, C.-L. Ho, H. Nishihara and W.-Y. Wong, *J. Mater. Chem. C*, 2019, **7**, 9159–9166.
152 F. Yu, W. Liu, S.-W. Ke, M. Kurmoo, J.-L. Zuo and Q. Zhang, *Nat. Commun.*, 2020, **11**, 1–6.
153 Y. Wang, Y. Wu, Y. Huang, F. Zhang, X. Yang, Y. Ma and Y. Chen, *J. Phys. Chem. C*, 2011, **115**, 23192–23197.
154 X. Yang, J. Zhu, L. Qiu and D. Li, *Adv. Mater.*, 2011, **23**, 2833–2838.
155 K. Zhang, N. Li, Y. Wang, X. Ma, J. Zhao, L. Qiang, S. Hou, J. Ji and Y. Li, *J. Mater. Sci.: Mater. Electron.*, 2018, **29**, 14803–14812.
156 K. Tang, Y. Zhang, Y. Shi, J. Cui, X. Shu, Y. Wang, Y. Qin, J. Liu, H. H. Tan and Y. Wu, *Electrochim. Acta*, 2020, **330**, 135189.
157 R. Giannuzzi, R. Scarfiello, T. Sibillano, C. Nobile, V. Grillo, C. Giannini, P. D. Cozzoli and M. Manca, *Nano Energy*, 2017, **41**, 634–645.
158 J. Li, Q. Guo, Y. Lu and G. Nie, *Eur. Polym. J.*, 2019, **113**, 29–35.
159 G. K. Ong, C. A. Saez Cabezas, M. N. Dominguez, S. L. Skjærvø, S. Heo and D. J. Milliron, *Chem. Mater.*, 2019, **32**, 468–475.
160 G. Cai, P. Cui, W. Shi, S. Morris, S. N. Lou, J. Chen, J. H. Ciou, V. K. Paidi, K. S. Lee, S. Li and P. S. Lee, *Adv. Sci.*, 2020, **7**, 1903109.
161 X. Qu, Y. Fu, C. Ma, Y. Yang, D. Shi, D. Chu and X. Yu, *New J. Chem.*, 2020, **44**, 15475–15482.
162 S. Mishra, S. Lambora, P. Yogi, P. R. Sagdeo and R. Kumar, *ACS Appl. Nano Mater.*, 2018, **1**, 3715–3723.
163 H. Lv, Y. Wang, L. Pan, L. Zhang, H. Zhang, L. Shang, H. Qu, N. Li, J. Zhao and Y. Li, *Phys. Chem. Chem. Phys.*, 2018, **20**, 5818–5826.
164 H. Sun, W. Wang, Q. Fan, Y. Qi, Y. Xiong, Z. Jian and W. Chen, *Mater. Sci. Semicond. Process.*, 2023, **155**, 107265.
165 S. Zhao, B. Wang, Y. Huang, Y. Zhang, X. Wu, Q. Jiang, D. Gao, F. Wang, R. Li, Y. Li, Y. Zhao, J. Li and R. Zhang, *ACS Appl. Nano Mater.*, 2023, **6**, 15021–15028.
166 B. Zhuang, Q. Zhang, K. Zhou and H. Wang, *RSC Adv.*, 2023, **13**, 18229–18237.
167 Z. Tong, X. Zhang, H. Lv, N. Li, H. Qu, J. Zhao, Y. Li and X. Y. Liu, *Adv. Mater. Interfaces*, 2015, **2**, 1500230.
168 D. Zhou, F. Shi, D. Xie, D. H. Wang, X. H. Xia, X. L. Wang, C. D. Gu and J. P. Tu, *J. Colloid Interface Sci.*, 2016, **465**, 112–120.
169 S. Mishra, P. Yogi, P. Sagdeo and R. Kumar, *ACS Appl. Energy Mater.*, 2018, **1**, 790–798.
170 D.-L. Sun, B.-W. Zhao, J.-B. Liu, H. Wang and H. Yan, *Ionics*, 2017, **23**, 1509–1515.
171 M. Rakibuddin, M. A. Shinde and H. Kim, *Electrochim. Acta*, 2020, 136403.
172 Y. Zhan, M. R. J. Tan, X. Cheng, W. M. A. Tan, G. F. Cai, J. W. Chen, V. Kumar, S. Magdassi and P. S. Lee, *J. Mater. Chem. C*, 2017, **5**, 9995–10000.
173 B. Lv, X. Liu, B. Yan, J. Deng, F. Gao, N. Chen and X. Wu, *Nanomaterials*, 2022, **12**, 1523.
174 M. Gugole, O. Olsson, K. Xiong, J. C. Blake, J. Montero Amenedo, I. Bayrak Pehlivan, G. A. Niklasson and A. Dahlin, *ACS Photonics*, 2020, 1762–1772.

175 T. Xu, E. C. Walter, A. Agrawal, C. Bohn, J. Velmurugan, W. Zhu, H. J. Lezec and A. A. Talin, *Nat. Commun.*, 2016, **7**, 10479.
176 M. Shahabuddin, T. McDowell, C. E. Bonner and N. Noginova, *ACS Appl. Nano Mater.*, 2019, **2**, 1713–1719.
177 A. Kristensen, J. K. Yang, S. I. Bozhevolnyi, S. Link, P. Nordlander, N. J. Halas and N. A. Mortensen, *Nat. Rev. Mater.*, 2016, **2**, 1–14.
178 Y. Lee, J. Yun, M. Seo, S.-J. Kim, J. Oh, C. M. Kang, H.-J. Sun, T. D. Chung and B. Lee, *Nano Lett.*, 2020, **20**, 6084–6090.
179 M. Atighilorestani, H. Jiang and B. Kaminska, *Adv. Opt. Mater.*, 2018, **6**, 1801179.
180 J. Peng, H.-H. Jeong, Q. Lin, S. Cormier, H.-L. Liang, M. F. De Volder, S. Vignolini and J. J. Baumberg, *Sci. Adv.*, 2019, **5**, eaaw2205.
181 C. Zhang, H. Subbaraman, Q. Li, Z. Pan, J. G. Ok, T. Ling, C.-J. Chung, X. Zhang, X. Lin and R. T. Chen, *J. Mater. Chem. C*, 2016, **4**, 5133–5153.
182 Y. Kuge, T. Ishinabe, Y. Shibata and H. Fujikake, *SID Symposium Digest of Technical Papers*, 2019, **50**, 267–270.
183 H. Yang, J.-H. Yu, H. J. Seo, R. H. Jeong and J.-H. Boo, *Appl. Surf. Sci.*, 2018, **461**, 88–92.
184 Y. Shi, M. Sun, Y. Zhang, J. Cui, Y. Wang, X. Shu, Y. Qin, H. H. Tan, J. Liu and Y. Wu, *Sol. Energy Mater. Sol. Cells*, 2020, **212**, 110579.
185 K. Lin, N. Jian, X. Zhang, Y. Zhang, S. Ming, S. Zhen, Q. Jiang, L. Wang, Y. Wang and J. Xu, *React. Funct. Polym.*, 2020, 104674.
186 L. Chen, X. Zhu, Y. Liu, L. Yang, J. Su, Z. He and B. Tang, *Electrochim. Acta*, 2024, **475**, 143644.
187 P. J. Morankar, R. U. Amate, A. M. Teli, S. A. Beknalkar and C.-W. Jeon, *Coatings*, 2024, **14**, 320.
188 X. Sun, D. Wang, W. Wu, X. Zhao, X. Zhang, B. Wang, X. Rong, G. Wu and X. Wang, *ACS Sustainable Chem. Eng.*, 2024, **12**, 5459–5467.
189 Y. Xiao, X. Zhang, D. Yan, J. Deng, M. Chen, H. Zhang, W. Sun, J. Zhao and Y. Li, *Nano Res.*, 2023, **17**, 3043–3052.
190 L. Zhao, Y. Zhu, X. Long, W. Liao, B. Hu, R. Miao, G. Zhang, G. Sun, Y. Xie and L. Miao, *Ceram. Int.*, 2024, **50**, 12810–12817.
191 A. K. Mak, Ö. Tuna, N. Sezgin, A. M. Üstün, Ş. Yılmaz, O. Öztürk and M. Karabulut, *Thin Solid Films*, 2022, **751**, 139241.
192 Y. Yin, C. Lan, S. Hu and C. Li, *J. Alloys Compd.*, 2018, **739**, 623–631.
193 E. Cazzanelli, M. Castriota, R. Kalendarev, A. Kuzmin and J. Purans, *Ionics*, 2003, **9**, 95–102.
194 J. Kilner and R. Brook, *Solid State Ionics*, 1982, **6**, 237–252.
195 G.-F. Cai, X.-L. Wang, D. Zhou, J.-H. Zhang, Q.-Q. Xiong, C.-D. Gu and J.-P. Tu, *RSC Adv.*, 2013, **3**, 6896–6905.
196 J. Hou, L. Gao, X. Gu, Z. Li, M. Huang and G. Su, *Mater. Chem. Phys.*, 2023, **306**, 128079.
197 D. Mohanadas, N. I. A. Zainudin and Y. Sulaiman, *Chem. Eng. J.*, 2022, **428**, 130989.
198 M. Hassan, A. Ghaffar, G. Lou, Z. Miao, Z. Peng and K. Celebi, *Adv. Funct. Mater.*, 2024, 2310535.
199 C. Wang, G. Dong, Y. Zhao, Y. He, Y. Ding, X. Du, X. Zhong, M. Wang and X. Diao, *J. Alloys Compd.*, 2020, **821**, 153365.
200 Q. Huang, Q. Zhang, Y. Xiao, Y. He and X. Diao, *J. Alloys Compd.*, 2018, **747**, 416–422.
201 K. Shen, K. Sheng, Z. Wang, J. Zheng and C. Xu, *Appl. Surf. Sci.*, 2020, **501**, 144003.
202 I. Mjejri, M. Gaudon and A. Rougier, *Sol. Energy Mater. Sol. Cells*, 2019, **198**, 19–25.
203 A. Chaudhary, D. K. Pathak, M. Tanwar, P. R. Sagdeo and R. Kumar, *ACS Appl. Electron. Mater.*, 2019, **1**, 892–899.
204 D. K. Pathak, A. Chaudhary, M. Tanwar, U. K. Goutam and R. Kumar, *Appl. Phys. Lett.*, 2020, **116**, 141901.
205 B. N. Reddy, P. N. Kumar and M. Deepa, *ChemPhysChem*, 2015, **16**, 377–389.
206 H. Li, L. McRae and A. Y. Elezzabi, *ACS Appl. Mater. Interfaces*, 2018, **10**, 10520–10527.
207 M. Ciobanu, J. Klein, M. Middendorf, S. M. B. Mousavi, F. Carl, M. Haase and L. Walder, *Sol. Energy Mater. Sol. Cells*, 2019, **203**, 110186.
208 K. Zhang, N. Li, X. Ma, Y. Wang, J. Zhao, L. Qiang, X. Li and Y. Li, *J. Electroanal. Chem.*, 2018, **825**, 16–21.
209 P. Yilmaz, M. Magni, S. Martinez, R. M. Gonzalez Gil, M. Della Pirriera and M. Manca, *ACS Appl. Energy Mater.*, 2020, **3**, 3779–3788.
210 T. Lin, W. Liu, B. Yan, J. Li, Y. Lin, Y. Zhao, Z. Shi and S. Chen, *Nanomaterials*, 2021, **11**, 2956.
211 J. Han, K.-W. Ko, S. Sarwar, M.-S. Lee, S. Park, S. Hong and C.-H. Han, *Electrochim. Acta*, 2018, **278**, 396–404.
212 N. Usha, R. Sivakumar and C. Sanjeeviraja, *Mater. Lett.*, 2018, **229**, 189–192.
213 M. Meenakshi, R. Sivakumar, P. Perumal and C. Sanjeeviraja, *Mater. Today: Proc.*, 2016, **3**, S30–S39.
214 C. A. Saez Cabezas, K. Miller, S. Heo, A. Dolocan, G. LeBlanc and D. J. Milliron, *Chem. Mater.*, 2020, 4600–4608.
215 Y. S. Nam, H. Park, A. P. Magyar, D. S. Yun, T. S. Pollom Jr. and A. M. Belcher, *Nanoscale*, 2012, **4**, 3405–3409.
216 S. Ming, Z. Li, J. Wang, H. Zhang and J. Zhao, *Chem. Eng. J.*, 2024, **479**, 147623.
217 H. C. Lu, S. Y. Kao, H. F. Yu, T. H. Chang, C. W. Kung and K. C. Ho, *ACS Appl. Mater. Interfaces*, 2016, **8**, 30351–30361.
218 W.-N. Wu, H.-F. Yu, M.-H. Yeh and K.-C. Ho, *Sol. Energy Mater. Sol. Cells*, 2020, **208**, 110375.
219 H.-S. Liu, B.-C. Pan, D.-C. Huang, Y.-R. Kung, C.-M. Leu and G.-S. Liou, *NPG Asia Mater.*, 2017, **9**, e388–e388.
220 Y. Zhou, X. Liu, X. Jia and D. Chao, *Eur. Polym. J.*, 2019, **111**, 43–48.
221 M. Jamdegni and A. Kaur, *J. Electrochem. Soc.*, 2019, **166**, H502.
222 S. Zhang, S. Chen, Y. Zhao, J. Kang, J. Chen, B. Yan, Y. Gu, F. Yang and Y. Cao, *J. Electrochem. Soc.*, 2019, **166**, H77.

223 S. Zhang, S. Chen, Y. Cao, F. Yang, H. Peng, B. Yan, H. Jiang, Y. Gu and M. Xiang, *J. Mater. Sci.: Mater. Electron.*, 2019, **30**, 13497–13508.
224 A. Llordés, G. Garcia, J. Gazquez and D. J. Milliron, *Nature*, 2013, **500**, 323–326.
225 Q. Wang, S. Cao, Q. Meng, K. Wang, T. Yang, J. Zhao and B. Zou, *Mater. Horiz.*, 2023, **10**, 960–966.
226 S. Heo, C. J. Dahlman, C. M. Staller, T. Jiang, A. Dolocan, B. A. Korgel and D. J. Milliron, *Nano Lett.*, 2020, **20**, 2072–2079.
227 SageGlass Saint-Gobain, **https://www.sageglass.com/**, (accessed 17/10/24, 2024).
228 Smart Windows for Smart buildings | View Smart Windows, **https://view.com/**, (accessed 17/10/24, 2024).
229 Kinestral, **https://archello.com/brand/kinestral-technologies**, (accessed 08/04/2025, 2025).
230 IQglass, **https://www.iqglassuk.com/**, (accessed 08/04/2025, 2025).
231 Strait research, **https://straitsresearch.com/report/electrochromic-glass-market**, (accessed 08/04/2025, 2025).
232 Z. Zhou, Z. Chen, D. Ma and J. Wang, *Sol. Energy Mater. Sol. Cells*, 2023, **253**, 112226.
233 B. Deng, Y. Zhu, X. Wang, J. Zhu, M. Liu, M. Liu, Y. He, C. Zhu, C. Zhang and H. Meng, *Adv. Mater.*, 2023, **35**, 2302685.
234 C. Park, J. M. Kim, Y. Kim, S. Bae, M. Do, S. Im, S. Yoo and J. H. Kim, *ACS Appl. Electron. Mater.*, 2021, **3**, 4781–4792.
235 Z. Wang, X. Jia, P. Zhang, Y. Liu, H. Qi, P. Zhang, U. Kaiser, S. Reineke, R. Dong and X. Feng, *Adv. Mater.*, 2022, **34**, 2106073.
236 M. Son, D. Shin and C. S. Lee, *Adv. Mater. Interfaces*, 2021, **8**, 2001416.
237 X. Tang, J. Chen, Z. Wang, Z. Hu, G. Song, S. Zhang, Z. Chen, Q. Wu, M. Liu, S. Cong and Z. Zhao, *Adv. Opt. Mater.*, 2021, **9**, 2100637.
238 G. T. Phan, D. V. Pham, R. A. Patil, C.-H. Tsai, C.-C. Lai, W.-C. Yeh, Y. Liou and Y.-R. Ma, *Sol. Energy Mater. Sol. Cells*, 2021, **231**, 111306.
239 S. Grewal, T. G. Habteyes, W. M. Takele, D. Chen, J. K. Grey and N. T. Hahn, *ACS Appl. Opt. Mater.*, 2024, **2**, 361–367.
240 J. Guay, R. Paynter and L. H. Dao, *Macromolecules*, 1990, **23**, 3598–3605.
241 H. Zhang, J. Feng, F. Sun, D. Zhou, G. Cao, S. Wang, X. Hu, J. Ma, F. Su, Y. Tian and Y. Tian, *Adv. Mater. Technol.*, 2023, **8**, 2201688.
242 J.-L. Wang, S.-Z. Sheng, Z. He, R. Wang, Z. Pan, H.-Y. Zhao, J.-W. Liu and S.-H. Yu, *Nano Lett.*, 2021, **21**, 9976–9982.
243 C. S. Ah, J. Song, S. M. Cho, T. Y. Kim, H. Ryu, S. Cheon, S. Kim, J. Y. Kim, Y. H. Kim and C. S. Hwang, *Bull. Korean Chem. Soc.*, 2018, **39**, 1186–1192.
244 H. N. Kim, S. M. Cho, C. S. Ah, J. Song, H. Ryu, Y. H. Kim and T.-Y. Kim, *Mater. Res. Bull.*, 2016, **82**, 16–21.
245 K. Tajima, H. Hotta, Y. Yamada, M. Okada and K. Yoshimura, *Appl. Phys. Lett.*, 2012, **100**, 091906.
246 Ray Ban Meta AR-AI glasses | Meta Store, **https://www.meta.com/au/ai-glasses/?utm_source=about.fb.com&utm_medium=organicsearch**, (accessed 12/12/24, 2024).
247 M. Gurman, Samsung Set to Enter AR Glasses Market in Race With Meta, Apple, **https://www.bnnbloomberg.ca/business/technology/2025/01/22/samsung-set-to-enter-ar-glasses-market-in-race-with-meta-apple/**.
248 T. Bajarin, How Smart Glasses From Apple Could Reshape The Market, **https://www.forbes.com/sites/timbajarin/2025/03/11/how-smart-glasses-from-apple-could-reshape-the-market/**.
249 Meta has launched the world's 'most advanced' glasses. Will they replace smartphones?, **https://theconversation.com/meta-has-launched-the-worlds-most-advanced-glasses-will-they-replace-smartphones-240023**, (accessed 08/04/2025, 2025).
250 A. L.-S. Eh, J. Chen, S. H. Yu, G. Thangavel, X. Zhou, G. Cai, S. Li, D. H. C. Chua and P. S. Lee, *Adv. Sci.*, 2020, **7**, 1903198.
251 Gentex Corporation, **https://www.gentex.com/products-technology/automotive/dimmable-glass/**, (accessed 10/03/2025, 2025).
252 Y. Wang, X. Zhong, X. Liu, Z. Lu, Y. Su, M. Wang and X. Diao, *J. Mater. Chem. A*, 2022, **10**, 3944–3952.
253 Q. Huang, J. Wang, H. Gong, Q. Zhang, M. Wang, W. Wang, J. P. Nshimiyimana and X. Diao, *J. Mater. Chem. A*, 2021, **9**, 6451–6459.
254 D. K. Pathak and H. C. Moon, *Mater. Horiz.*, 2022, **9**, 2949–2975.
255 Y. Zhong, X. Xia, W. Mai, J. Tu and H. J. Fan, *Adv. Mater. Technol.*, 2017, **2**, 1700182.
256 S. Zhang, J. Ren, Y. Zhang, H. Peng, S. Chen, F. Yang and Y. Cao, *Org. Electron.*, 2020, **77**, 105497.
257 K.-W. Kim, T. Y. Yun, S.-H. You, X. Tang, J. Lee, Y. Seo, Y.-T. Kim, S. H. Kim, H. C. Moon and J. K. Kim, *NPG Asia Mater.*, 2020, **12**, 84.
258 Y. Sun, X. Zhao, G. Zhu, M. Li, X. Zhang, H. Yang and B. Lin, *Electrochim. Acta*, 2020, **333**, 135495.
259 K. Zhou, H. Wang, J. Jiu, J. Liu, H. Yan and K. Suganuma, *Chem. Eng. J.*, 2018, **345**, 290–299.
260 T. G. Yun, M. Park, D. H. Kim, D. Kim, J. Y. Cheong, J. G. Bae, S. M. Han and I. D. Kim, *ACS Nano*, 2019, **13**, 3141–3150.
261 J. Chen, Z. Wang, Z. Chen, S. Cong and Z. Zhao, *Nano Lett.*, 2020, **20**, 1915–1922.
262 H. Li, C. J. Firby and A. Y. Elezzabi, *Joule*, 2019, **3**, 2268–2278.
263 W. Zhang, H. Li, M. Al-Hussein and A. Y. Elezzabi, *Adv. Opt. Mater.*, 2020, **8**, 1901224.
264 X. Yu, M. Chang, W. Chen, D. Liang, X. Lu and G. Zhou, *ACS Appl. Mater. Interfaces*, 2020, **12**, 39505–39514.
265 W. Wu, H. Fang, H. Ma, L. Wu, Q. Wang and H. Wang, *ACS Appl. Mater. Interfaces*, 2021, **13**, 20326–20335.

266 W. Zhang, H. Li and A. Y. Elezzabi, *Adv. Funct. Mater.*, 2022, **32**, 2108341.
267 W. Zhang, H. Li, W. W. Yu and A. Y. Elezzabi, *Light: Sci. Appl.*, 2020, **9**, 121.
268 S. Bi, W. Jin, X. Han, X. Cao, Z. He, K. Asare-Yeboah and C. Jiang, *Nano Energy*, 2022, **102**, 107629.
269 G. Liu, Z. Wang, J. Wang, H. Liu and Z. Li, *J. Colloid Interface Sci.*, 2024, **655**, 493–507.
270 Z. Wu, Q. Zhao, X. Luo, H. Ma, W. Zheng, J. Yu, Z. Zhang, K. Zhang, K. Qu, R. Yang, N. Jian, J. Hou, X. Liu, J. Xu and B. Lu, *Chem. Mater.*, 2022, **34**, 9923–9933.
271 M. Aller-Pellitero, S. Santiago-Malagón, J. Ruiz, Y. Alonso, B. Lakard, J.-Y. Hihn, G. Guirado and F. J. del Campo, *Sens. Actuators, B*, 2020, **306**, 127535.
272 D. K. Pathak, A. Chaudhary, M. Tanwar, U. K. Goutam, P. Mondal and R. Kumar, *ACS Appl. Nano Mater.*, 2021, **4**, 2143–2152.
273 S. Y. Yeon, M. Seo, Y. Kim, H. Hong and T. D. Chung, *Biosens. Bioelectron.*, 2022, **203**, 114002.
274 D. S. Kim, Y. H. Lee, J. W. Kim, H. Lee, G. Jung and J. S. Ha, *Chem. Eng. J.*, 2022, **429**, 132289.
275 S. Santiago-Malagón, D. Río-Colín, H. Azizkhani, M. Aller-Pellitero, G. Guirado and F. J. del Campo, *Biosens. Bioelectron.*, 2021, **175**, 112879.
276 A. P. M. Tavares, L. Truta, F. T. C. Moreira, G. Minas and M. G. F. Sales, *Biosens. Bioelectron.*, 2019, **137**, 72–81.
277 X. Wang, W. Yuan, Z. Sun, F. Liu and D. Wang, *Food Chem.*, 2023, **403**, 134240.
278 S. Ranjbar, M. A. F. Nejad, C. Parolo, S. Shahrokhian and A. Merkoçi, *Anal. Chem.*, 2019, **91**, 14960–14966.
279 D. Yu, H. Zhang, L. Bai, Y. Fang, C. Liu, H. Zhang, T. Li, L. Han, Y. Yu, H. Yu and S. Dong, *Sens. Actuators, B*, 2020, **302**, 127177.
280 K. Chen, J. He, D. Zhang, L. You, X. Li, H. Wang and J. Mei, *Nano Lett.*, 2021, **21**, 4500–4507.
281 R. Zheng, Y. Wang, C. Jia, Z. Wan, J. Luo, H. A. Malik, X. Weng, J. Xie and L. Deng, *ACS Appl. Mater. Interfaces*, 2018, **10**, 35533–35538.
282 J. Koo, V. Amoli, S. Y. Kim, C. Lee, J. Kim, S.-M. Park, J. Kim, J. M. Ahn, K. J. Jung and D. H. Kim, *Nano Energy*, 2020, **78**, 105199.
283 K. Li, Y. Shao, H. Yan, Z. Lu, K. J. Griffith, J. Yan, G. Wang, H. Fan, J. Lu, W. Huang, B. Bao, X. Liu, C. Hou, Q. Zhang, Y. Li, J. Yu and H. Wang, *Nat. Commun.*, 2018, **9**, 4798.
284 E. Detsi, P. Onck and J. T. M. De Hosson, *Appl. Phys. Lett.*, 2013, **103**, 193101.
285 N. O. Laschuk, I. I. Ebralidze, E. B. Easton and O. V. Zenkina, *ACS Appl. Mater. Interfaces*, 2021, **13**, 39573–39583.
286 X. Zhang, Y. Yang, P. Xue, C. Valenzuela, Y. Chen, X. Yang, L. Wang and W. Feng, *Angew. Chem., Int. Ed.*, 2022, **61**, e202211030.
287 M. Beregoi, C. Busuioc, A. Evanghelidis, E. Matei, F. Iordache, M. Radu, A. Dinischiotu and I. Enculescu, *Int. J. Pharm.*, 2016, **510**, 465–473.
288 W.-Q. Wang, X.-L. Wang, X.-H. Xia, Z.-J. Yao, Y. Zhong and J.-P. Tu, *Nanoscale*, 2018, **10**, 8162–8169.
289 G. Cai, P. Darmawan, X. Cheng and P. S. Lee, *Adv. Energy Mater.*, 2017, **7**, 1602598.
290 G. Cai, X. Wang, M. Cui, P. Darmawan, J. Wang, A. L.-S. Eh and P. S. Lee, *Nano Energy*, 2015, **12**, 258–267.
291 X. Xia, Z. Ku, D. Zhou, Y. Zhong, Y. Zhang, Y. Wang, M. J. Huang, J. Tu and H. J. Fan, *Mater. Horiz.*, 2016, **3**, 588–595.
292 Y. Wang, H. Jiang, R. Zheng, J. Pan, J. Niu, X. Zou and C. Jia, *J. Mater. Chem. A*, 2020, **8**, 12799–12809.
293 Y. Zhu, T. Tsukamoto and S. Tanaka, *J. Micromech. Microeng.*, 2017, **27**, 125012.
294 D. Capoferri, R. Alvarez-Diduk, M. Del Carlo, D. Compagnone and A. Merkoci, *Anal. Chem.*, 2018, **90**, 5850–5856.
295 D. Yu, H. Zhang, L. Bai, Y. Fang, C. Liu, H. Zhang, T. Li, L. Han, Y. Yu and H. Yu, *Sens. Actuators, B*, 2020, **302**, 127177.